Refining Molecular Beam Techniques for Enhanced State-Selective Ionization of N_2^+

Master's Thesis

submitted to

Indian Institute of Science Education and Research Tirupati

in partial fulfillment of the requirements for the

BS-MS Dual Degree Programme

by

Rukmini Parashram Harale
Roll Number: 20191116

Supervisor: Dr. Ziv Meir
Department of Physics of Complex Systems of
Weizmann Institute of Science, Israel

April, 2024

Certificate

This is to certify that the MS Thesis entitled 'Refining Molecular Beam Techniques for Enhanced State-Selective Ionization of N_2^+', submitted towards the partial fulfillment of the BS-MS dual degree programme at the Indian Institute of Science Education and Research Tirupati, represents the study/work carried out by Rukmini Parashram Harale at External Institute Weizmann Institute of Science, Israel under the supervision of Dr. Ziv Meir, Department of Physics of Complex Systems, during the academic year 2023-2024 and the same has not been submitted for any other degree or diploma of any other university or institute.

Name of a Student: Rukmini Parashram Harale
Roll Number: 20191116

Signature of Student:
Date:

Name of a Supervisor: Dr. Ziv Meir

Signature of Supervisor:
Date:

Declaration

I declare that the matter presented in the MS thesis entitled 'Refining Molecular Beam Techniques for Enhanced State-Selective Ionization of N_2^+,' are the results of the work carried out by me at the Department of Physics of Complex Systems, Weizmann Institute of Science, Israel, under the supervision of Dr. Ziv Meir. I declare that the study/work submitted is my own and expressed in my own words. My contributions and those of the other collaborators (if any) to this work have been explicitly indicated below. I confirm that appropriate credit has been given within this thesis where reference has been made to the work of others. I also declare that I have adhered to all principles of academic ethics and integrity and have not fabricated or falsified any idea/data/fact/image source in my submission. I understand that violation of the above will lead to disciplinary action by the Institute and can also evoke penal action from the sources which have thus not been properly cited or from whom proper permission has not been obtained.

Name of a Student: Rukmini Parashram Harale
Roll Number: 20191116

Signature of Student:
Date:

Endorsed by
Name of a Supervisor: Dr. Ziv Meir

Signature of Supervisor:
Date:

Acknowledgments

Embarking on the adventure of my Master's thesis felt less like stepping into the academic unknown and more like joining a band of merry scholars, thanks to the cast of characters who've made this journey unforgettable. At the helm was my advisor, Ziv, possibly the world's most affable guide through the maze of research. His superpower? Making the pressure of work feel like a light breeze, ensuring that academic pursuit felt less like labor and more like a labor of love. A standing ovation is due for Idan, the saint of patience, who faced the same question a thousandth of the time and still answered with remarkable fortitude and unwavering grace. I am grateful to Osip Schwartz for his willingness to be my TAC member and for his constructive feedback and support.

I want to thank the technical and administrative staff in the Department of Physics of Complex Systems, particularly Malka and Debbie, who smoothed out every bureaucratic bump, making paperwork seem like paper planes. And then there's Guy with a meme collection in his office and a treasure trove of screws and his help in making homemade parts for our experiment. Yossi showed me that laser-fixing could be as delightful as a cup of tea with a friend, proving that age is but a number when it comes to camaraderie.

I acknowledge the academic program at IISER for giving me an opportunity and providing the necessary facilities to work on my research outside my institution. Their Support has played a crucial role in my academic pursuits.

I'm grateful to Tamar, Katarina, and Jonas, who made my initial days a breeze, leaving behind shoes too big to fill, promptly occupied by Mai and चिड़िया aka Mafkir ~~Dror~~. These two turned our office into a den of joy, and under their snack siege, my desk resembled a bustling kiosk more than a workspace. A shoutout to my other lab mates - Tom and Orr - whose support was as steady as a rock and to Akash, my best friend, who, despite time zones, was always just a call away, ensuring loneliness stayed a stranger. And to the pillars of my life, my parents, whose unwavering support and teachings have sculpted me. To Bapuji, for his genuine interest in all my endeavors, coupled with the values of curiosity and critical thinking he has instilled in me, have shaped the person I am today.

This thesis, a mosaic of learning, laughter, and the occasional laser mishap stands as a tribute to all of you. Here's to the collective effort, the shared giggles, and the countless snack and extended coffee breaks that fueled this academic odyssey. My deepest, most heartfelt thanks to each and every one of you for

adding color, laughter, and knowledge to this chapter of my life.

Abstract

The quest for precision and control at a quantum level continues to challenge and inspire researchers. It is a prerequisite for quantum control to have a high-fidelity state preparation. We are working to improve our molecular-ion state preparation by state-selective ionization using resonance-enhanced multi-photon ionization (REMPI). We demonstrated the ionization scheme given by Mackenzie et al. [1], and we found the ionization threshold at $125625cm^{-1}$, which is shifted from the theoretical value due to a non-vanishing electric field in the ionization region. To avoid this shift, we developed an HV switch to mitigate the effect of the DC electric field from the Time-Of-Flight Mass Spectrometer (TOF-MS) on the ionization energy. We also developed a new approach for loading calcium through the molecular beam, and for that, we designed a home-built oven and tested it in our experiment. With these upgrades to our existing molecular beam setup, we hope to achieve better quantum-state selectivity and improve our ability to conduct experiments with trapped molecular ions. Due to unforeseen circumstances, we had a small detour, where we delved into investigating the application of confining two masses with a significant mass difference in a dual-frequency trap. In this thesis, we simulated the behavior of two ions trapped in a single-frequency trap, which aligns with the theoretical predictions.

Contents

Contents **8**

List of Figures **10**

1 Introduction **11**
1.1 Nitrogen molecule 12
1.2 Supersonic expansion 13
1.3 REMPI 15
1.4 TOF-MS 16

2 Experimental System **19**
2.1 Vacuum setup 19
2.2 Laser System 21
2.3 Control hardware 22

3 Results **24**
3.1 REMPI 24
3.1.1 Time-of-flight of N_2^+ 24
3.1.2 2+1 REMPI spectrum 26
3.1.3 2+1' REMPI 27
3.2 HV Switch 28
3.2.1 Testing of the switch 28
3.2.2 Assembly 29
3.3 Calcium oven 30
3.3.1 Design 30
3.3.2 Cleaning 30
3.3.3 Testing of the oven 31
3.3.4 Preliminary searches for Ca^+ TOF-MS signal 31

4 Dual Frequency **34**
4.1 Generic paul trap 34

4.2 Dual-frequency Paul trap 40

5 Discussion **41**

Bibliography **43**

A Code for Simulation of Dual-frequency **46**
A.1 Simulation of one ion in a trap 46
A.2 Simulation of two ions in a trap 50
A.3 Simulation of two ions in Dual-frequency Paul trap 57

B Meme **61**

List of Figures

1.1 Schematic of the energy level of N_2^+ in its electronic ground state . . . 14
1.2 REMPI methods for ionizing N_2 . . . 16
1.3 Schematic of Time-Of-Flight Electrodes . . . 18

2.1 Experimental Setup . . . 20
2.2 Pulse generation by OPX+ . . . 22

3.1 TOF Signal of N_2^+ . . . 25
3.2 TOF Simulation . . . 25
3.3 2+1 REMPI spectrum of N_2 . . . 26
3.4 Effect of Valve opening time on 2+1 REMPI spectrum . . . 27
3.5 2+1' REMPI Spectrum . . . 28
3.6 HV Switch Delay measurements . . . 29
3.7 HV Switch assembly . . . 29
3.8 Design of the home-built Ca oven . . . 31
3.9 Testing of the Ca oven . . . 32
3.10 2+1 REMPI Spectrum after installing the oven . . . 33

4.1 Paul Trap . . . 35
4.2 Comparison of computational and analytical solution of the motion of signal ion . . . 36
4.3 Frequency of the motion of a single ion trapped in a Paul trap . . . 37
4.4 Motion of two ions trapped in a Paul trap . . . 39

Chapter 1

Introduction

Quantum mechanics is where classical physics principles break down, and phenomena such as superposition and entanglement become prominent. The unique properties of quantum mechanics govern atomic and molecular structures marshaling our surroundings. Quantum information emerges as an evolutionary field from the profound principles of quantum mechanics and represents a paradigm shift in our understanding of information processing. However, that requires precise and coherent control of the system. Researchers have achieved this control on atomic ion systems[2]. A famous example is optical atomic clocks[3], which have revolutionized our ability to perform precision measurements.

Such a precise control has been demonstrated on molecules and molecular ions in the last few decades[4–7]. Molecules are advantageous over atoms due to their rich internal structures with multiple degrees of freedom and a wide range of mass and sizes. Their rich structure allows larger tunability, e.g., superpositions with enhanced coherence time. Polar molecules have a high susceptibility to electric fields, and microwave fields can drive internal rotational states. The rich internal structure of ultracold molecules, including many long-lived spins and rotational and vibrational levels, make them perfect candidates for 'qubits.' Molecules exhibit stronger and tunable interactions; coherently manipulating a quantum system of ultracold molecules ($\lesssim$1mK) with high precision can facilitate various quantum information applications, such as molecular metrology[8], quantum computing, quantum communication, quantum simulation[9], and many-body physics[10].

Quantum effects become more prominent at ultracold temperatures. However, cooling molecules is more complicated than cooling atoms. Atomic ions are generally laser-cooled to their ground state[11], which is impossible for most molecular ions due to their complex internal structure. Instead, molecular ions are sympathetically cooled by co-trapping them with a suitable laser-cooled ion[12]. How-

ever, sympathetic cooling cools only external degrees of freedom. One needs to use state-selective photoionization[13], buffer-gas cooling[14], or chemically bonding a cold atom with a neutral for cooling internal degrees of freedom[15, 16].

Considering the complexity of molecules, which allows a wider variety of interactions and the vast availability, they can be exploited in quantum simulations and quantum computing, metrology. Our research group aims to produce molecular qubits using N_2^+ molecules. As N_2^+ is a homonuclear molecule, electronic charge distribution is symmetric, resulting in a vanishing permanent dipole moment[17]. Due to zero dipole moment, rovibrational transitions are electric-dipole forbidden in the electronic ground state. Hence, N_2^+ is an ideal candidate for the implementation of qubits and clocks[9]. We use a home-built time-of-flight mass spectrometer (TOF-MS) to optimize the state-selective ionization of the N_2^+ molecule. We intend to use Ca^+ ions for sympathetic cooling of N_2^+ molecular ions and for molecular-state detection based on coherent motional excitation.

1.1 Nitrogen molecule

Homonuclear molecules like H_2 and N_2 typically do not exhibit an "infra-red" spectrum. Although this is true, it shows "electric-dipole-forbidden" transitions, which are spectrally extremely narrow. This intriguing phenomenon arises due to a quadrupole arrangement characterized by four regions with varying charge densities. This configuration resembles two spatially separated electric dipoles. When subjected to a uniform electric field, these dipoles oscillate nearly in phase, inducing nuclear vibration but not excitation. However, in general, an electromagnetic field has a phase shift over a molecule, which causes the dipoles to oscillate slightly out of phase, leading to vibrational excitation. Because the molecule's size is significantly smaller than the electromagnetic wavelength, the resulting phase shift remains minimal, resulting in weak electric-quadrupole vibrational transitions.

This unique behavior has sparked significant interest in high-precision measurements and precision spectroscopy. Until 2016, such transitions were exclusively observed in neutral molecules. However, Germann et al.,[18] reported on the observation of electric-quadrupole-rotation-vibration transitions in the Nitrogen molecular ion, N_2^+, directing new avenues for exploration in the field of molecular spectroscopy. Understanding these electric-quadrupole transitions offers profound insights into molecular dynamics and provides a deeper understanding of fundamental principles governing molecular behavior.

We are interested in the $X^2\Sigma_g^+$ electronic ground state of the N_2^+ molecular ion, which can be obtained from the $X^1\Sigma_g^+$ electronic ground state of the N_2 neutral molecule with an electronic configuration $1\sigma_g^2 1\sigma_u^2 2\sigma_g^2 2\sigma_u^2 3\sigma_g^2 1\pi_u^4$ by removing an electron from the $3\sigma_g$ orbital. The schematic of energy levels of the Nitrogen is shown in the 1.1. To obtain the nitrogen molecular ion, we use a Resonance-Enhanced Multi-Photon-Ionization (REMPI) scheme; for details, see section 1.3.

1.2 Supersonic expansion

High temperatures present a barrier to observing coherent phenomena that stem from the wave-like nature of particles, motivating the development of techniques for cooling matter to temperatures where macroscopic quantum behavior dominates. However, cooling molecules pose unique challenges due to their complex structures, as they lack suitable electronic transitions for direct laser cooling, which necessitates alternative methods based on collision mechanisms such as buffer-gas cooling, supersonic expansion, sympathetic cooling, and evaporation.

In supersonic expansion, the pulsed valve generates packets of cold molecules. The process exploits the hydrodynamic phenomenon of gas flowing from high pressure to vacuum to achieve natural cooling[19]. Initially, the gas is held at a small volume before the nozzle at temperature T_0 (300 K) and pressure P_0 (1-2 bar). When the nozzle (100 μm) opens, the gas enters the chamber, which is evacuated by a pump, maintaining a particular background pressure P_b (10^{-8} mbar). Values in apprentices are our own typical experimental values. As the gas flows from the higher pressure P_0 to the lower pressure P_b, it accelerates, and subsequent expansion occurs until the flow meets the boundary condition imposed by the background pressure P_b. This results in decreased enthalpy, which follows the cooling of the gas to lower temperatures. The process is ideally isentropic but cannot produce a complete ensemble with a low spread of momentum vectors everywhere solely through expansion. Instead, the velocity magnitude becomes uniform while the spread of momentum vectors is small.

We use the state-selective ionization in our experiment(for more details, see section 1.3), which is more effective when molecules are sufficiently cold, and the ground state population is maximal. Thus to produce molecules with narrow energy distributions, we use the supersonic expansion.

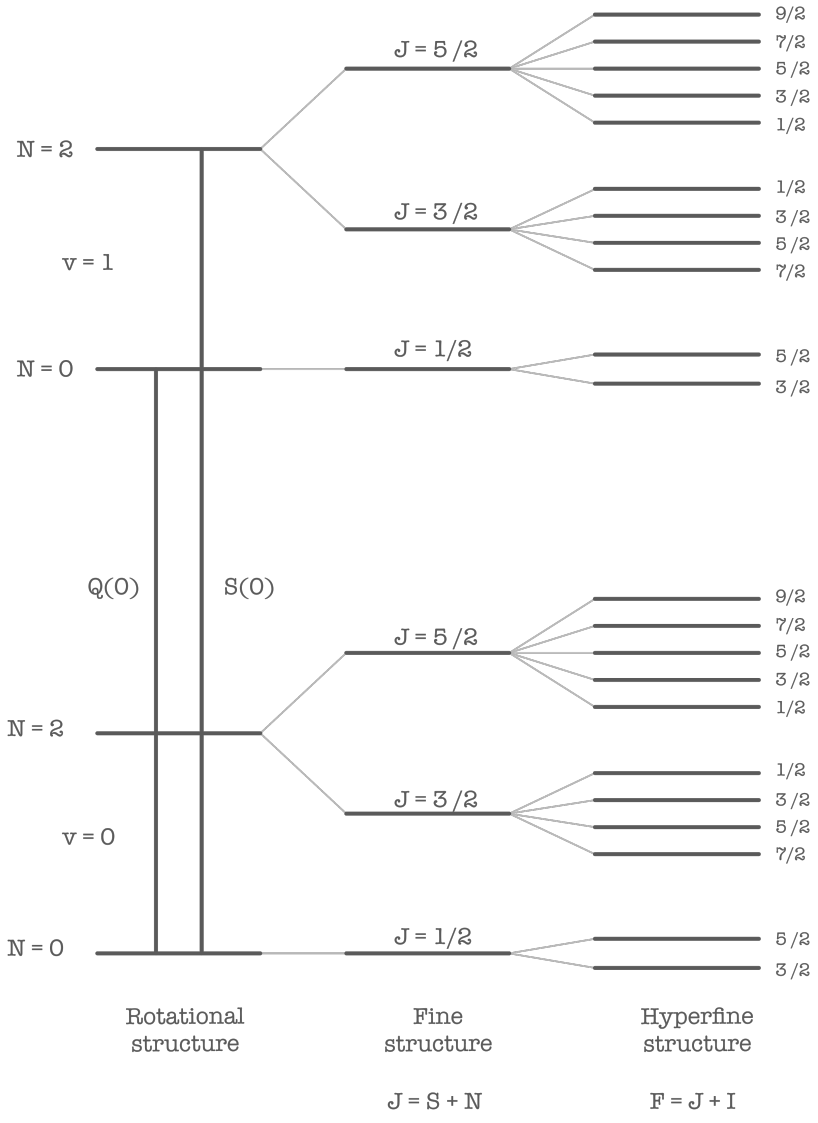

Figure 1.1: This is schematic of the energy level of N_2^+ in its electronic ground state (not to scale) [9]. N denotes the rotational level. For $N > 0$, the levels split into spin-rotation component($J = N \pm S$, where $S = 1/2$). The energy levels further split into hyperfine structures due to the interaction with nuclear spin ($|J - I| < F < J + I$, where I = 2)

1.3 REMPI

Resonance-enhanced multi-photon ionization (REMPI) is a versatile technique used in spectroscopy and quantum-state preparation. A fundamental step in creating a qubit is preparing it in a definite state. This is done in our experiment by ionizing neutral molecules to the desired state of the ion. REMPI, with its control over quantum states through laser manipulation, offers a valuable tool for precisely preparing and manipulating quantum states. The REMPI is associated with the photoabsorption of two or more photons [20].

In REMPI, the molecule absorbs photons matched to the energy gap between its ground and excited states, thereby ensuring that the ionization process taps directly into the molecular spectroscopy of the species in question. This "resonance-enhanced" absorption is followed by the absorption of additional photons that lead to ionization. The selectivity of the REMPI process comes from the fact that molecular spectroscopy is directly involved in the ionization process. One common REMPI process is the 2+1 REMPI, where a two-photon process is used to excite the intermediate neutral state. Its efficiency is fundamentally proportional to the square of the light intensity, a parameter that is impracticably small with conventional light sources. However, modern pulsed lasers evade this issue by producing a high photon density, making ionization efficiencies of 10% or greater feasible [20], especially where the overlap between the laser and molecular gas beams is maximal.

Nitrogen cation (N_2^+) has garnered interest for quantum control experiments due to its symmetric structure and low reactivity, making it a good candidate for studying the dynamics of quantum-state preparation via REMPI. Different 2+1' REMPI ionization processes have been employed for N_2^+, as showcased in the works of Mackenzie et al.[1] and Gardner et al. [21] (Figure 1.2). Mackenzie et al.[1] uses 202nm photons to excite N_2 to an intermediate state and then ionize it to N_2^+ using 375nm photons. However, the 2+1 ionization in this scheme using only 202nm photons is not state-selective. The non-selective part will significantly contribute as this wavelength is more energetic than 375 nm. An alternative approach, proposed by Gardner et al.[21], suggests using uses 255nm photons to excite N_2 to an intermediate state and then ionize it to N_2^+ using 212nm photon. A single-color, 2+1, non-selective process is energetically forbidden in this scheme. For that, state selectivity is expected to improve with this scheme.

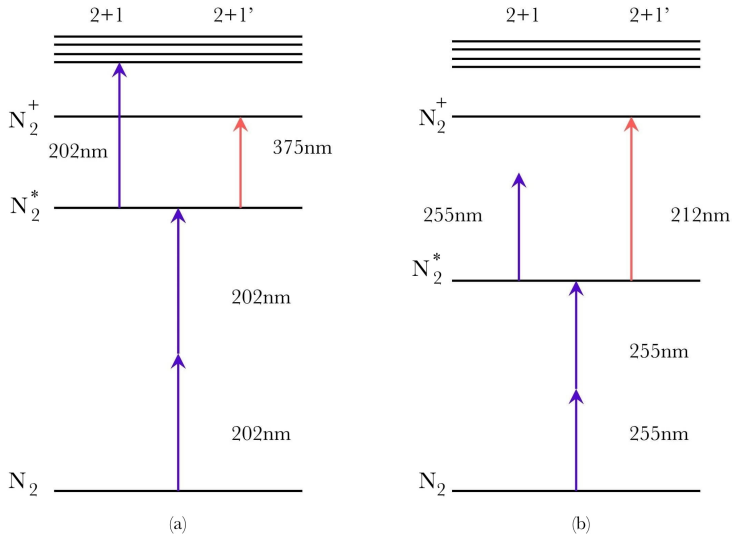

Figure 1.2: REMPI methods for ionizing N_2.
(a) Mackenzie et al., $X^1\Sigma_g^+(\nu = 0) \longrightarrow a''^1\Sigma_g^+(\nu = 0) \longrightarrow X^2\Sigma_g^+(\nu = 0)$ [1].
(b) Gardner et al., $X^1\Sigma_g^+(\nu = 0) \longrightarrow a^1\Pi_g(\nu = 6) \longrightarrow X^2\Sigma_g^+(\nu = 0)$ [21].

1.4 TOF-MS

Time-Of-Flight Mass Spectrometry (TOF-MS) has taken a vital path in discovering isotopes of different elements, proving itself a pivotal technique in analytical chemistry. Today, it is a prevalent tool in many scientific disciplines. The fundamental idea of TOF-MS is that ion velocities disperse over time according to their different m/z ratios when subjected to the same potential energy. Mass analysis is based on the time of flight from ionization to detection.

Time dispersion in mass spectrometry was first introduced with the development of TOF-MS in 1946 by the groundbreaking work of Stephens [22]. However, they could achieve mass resolution of 20amu and 21amu only. In 1955, the groundbreaking work of W.C. Wiley and I.H. McLaren [23] introduced a revolutionary ion gun in a non-magnetic TOF-MS, improving mass resolution dramatically. They used a double-field ion source, which allowed for more precise control over ion acceleration by adjusting the separations and the electric fields of electrodes. It was achieved to maximize the focusing effect of the ion gun by analyzing the relationship between the initial spatial and kinetic energy distributions of the ions and their time of flight. This allowed the spectrometer to have a relative abundance of adjacent mass units well beyond the 100 atomic mass unit. It advanced the time of

flight analysis, offering high-resolution mass spectrum analysis with little physics restriction. However, there were still constraints on initial velocity and spatial dispersion, which Mamyrin [24] addressed in 1966 using the reflector, which delays the ion extraction and space focus approach. Deconstructing previous constraints, TOF-MS pushed to the mass resolution of 3000amu.

The measurement of ion flight duration demonstrates the principle of TOF-MS over a predetermined distance. It demonstrates the significant progress in enhancing the resolving power, sensitivity, and speed of TOF-MS compared to the developments in ion gating approaches and detecting systems. The employment of orthogonal acceleration and ion mirrors [24], among other innovations in spatial and energy-focusing techniques, has significantly improved the accuracy and efficiency of TOF-MS and allowed for high-resolution mass spectrometry over a broad mass range with lower ion loss. TOF-MS is based on two fundamental ideas. The first is the temporal focusing of particles with the same m/z ratio but different initial positions and momenta. The second is the differential acceleration of particles with various m/z ratios in static electric fields. Accelerated ions will focus at a specific time on a plane perpendicular to the accelerating field.

For our project, we use Wiley and McLaren's design [23] (see Figure 1.3). The distance between the repeller and the extractor electrodes is a, x is the distance from the position where the ion is formed, and the extractor electrode, b is the distance between the extractor and the accelerator electrodes, and c is the free-flight distance to the MCP detector. The time it takes to travel distance x, b, and c is t_x, t_b, t_c, respectively. a_a, a_b, a_c are the accelerations in the regions a, b, and c. V_{ext} is the potential on the extractor electrode, V_{rep} on the repeller, and V_{acc} on the accelerator electrode. Following this nomenclature,

$$a_a = \frac{z\,|V_{ext} - V_{rep}|}{ma}, \tag{1.1}$$

Where z is the charge on the ion and m is the mass of the ion. To avoid confusion, we take the absolute value of the voltage difference as the ion accelerates in the direction of the force. The initial velocity of the ion is assumed to be zero. The time ion takes to travel distance x,

$$t_x = \sqrt{\frac{2\,x}{a_a}}, \tag{1.2}$$

In the region between the extractor and the accelerator, the initial velocity will be governed by the acceleration from the previous region.

$$u_b = a_a t_a, \tag{1.3}$$

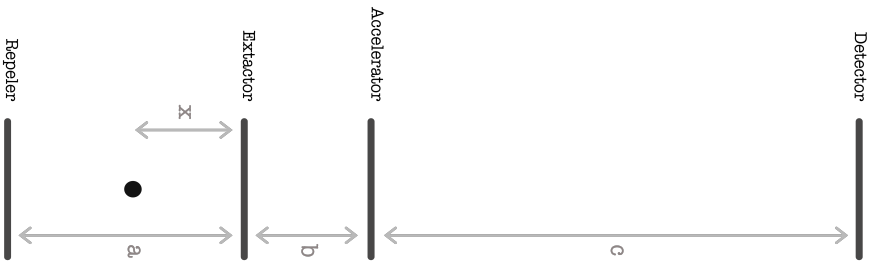

Figure 1.3: This schematic of a TOF-MS is based on a Wiley and McLaren design [23]. Ions are created between the repeller and extractor electrodes (the black dot) and accelerated towards the extractor due to electric field difference and further accelerated towards the accelerator. From there, ions perform a free flight until the detector.

The potential on the accelerator electrode is zero ($V_{acc} = 0$). Thus the acceleration in this region will be,

$$a_b = \frac{z\,|V_{ext}|}{mb}, \tag{1.4}$$

Using the Newtonian equations, we get the quadratic equation for the time t_b, but only one solution for t_b is possible as the other will give a negative time. Thus the time ion takes to travel distance b,

$$t_b = \frac{-u_b + \sqrt{u_b^2 + 2a_b b}}{a_b}, \tag{1.5}$$

For the free flight, the initial velocity will be

$$u_c = u_b + a_b t_b, \tag{1.6}$$

As there is no field, there will be zero acceleration, and the time taken by the ion to travel in this region will become,

$$t_c = c/u_c \tag{1.7}$$

The total time-of-flight of the ion will be,

$$t = t_x + t_b + t_c \tag{1.8}$$

Chapter 2

Experimental System

2.1 Vacuum setup

The experimental setup is core to the investigation of N_2^+ ion; it represents a realization of advancements and design considerations aimed at improving the capabilities of ion trapping and mass spectrometry analysis. The setup was mainly designed and built by Idan Hochner, a Ph.D. student in our group, before I arrived at the group. During my time in the group, I upgraded the system by adding two gate valves. The first valve was tactically placed to protect the Micro-Channel-Plate (MCP) detector during the venting process from potential contaminants in the air, and the other was required to attach the molecular beam to the ion-trapping setup to facilitate seamless integration between the two systems. Figure 2.1a shows the solid works design with the new upgrades for this experiment. In addition, I designed and built a Ca oven that is mounted on the pulsed valve to introduce calcium (not shown in Figure 2.1a). For more details about the oven, see section 3.3.

The foundation of the design is rooted in need for a highly controlled environment for producing and trapping ions. The setup is constructed as a dual-chamber vacuum system, integral for maintaining a high vacuum to minimize unwanted interactions with air or other contaminants. This clean environment is essential for the unrestrained operation of the molecular beam and ion-trapping mechanisms. The first chamber is maintained at a pressure of 10^{-8} mbar (pulsed valve is off) achieved by using an Edwards NEXT730D turbo-molecular pump and nXDS15i scroll pump. This chamber contains an Amsterdam Piezo Valve (APV) mounted on the XYZ stage, which can be controlled externally. Supersonic expansion through this pulsed valve provides a cold molecular beam with a narrow velocity distribution that is critical for our studies. The pressure in the valve chamber

typically increases to 10^{-5} mbar when the valve is open. The second chamber contains the home-built TOF-MS to detect ions. The TOF-MS was built according to Wiley and McLaren's design [25]. Both chambers are connected by a skimmer, which maintains differential pressure between the two chambers. This helps maintain the integrity of the pressure in the TOF-MS chamber (10^{-8} mbar), allowing uninterrupted mass spectrometer analysis. In addition, the skimmer collimates the molecular beam to the TOF chamber.

For the time-of-flight mass spectrometer, the electrodes are made of nickel metal grid spot welded on the stainless steel ring with distance a∼4 cm, b∼1 cm, c∼60 cm. The detector is the multi-channel-plate (MCP) (Photonis, chevron MCP 40-12-10-8 D 46:1). It can be tuned to 2kV, and the voltage on the anode is 2.5kV. The N_2 is ionized around x∼2 cm from the extractor electrode (see Figure 1.3).

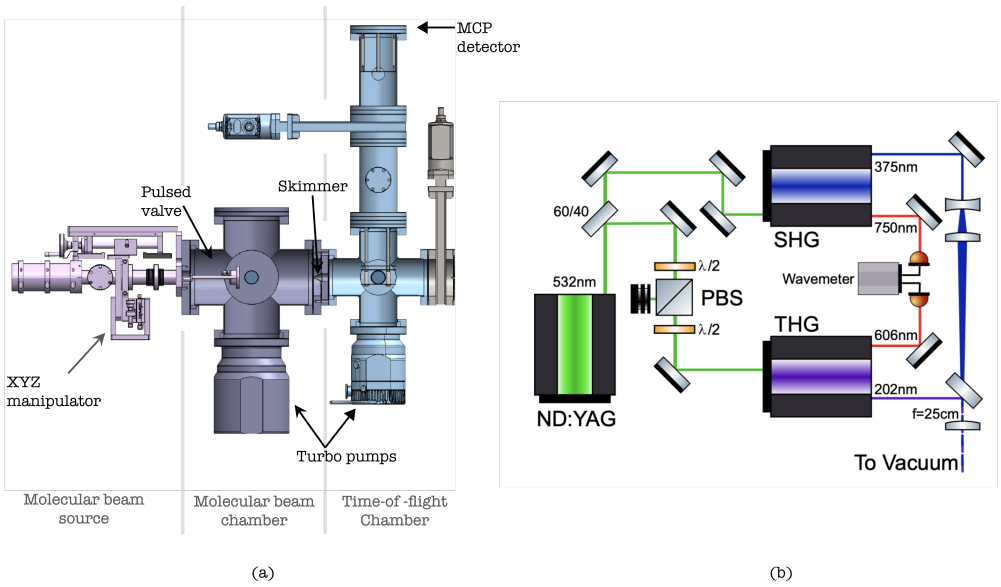

Figure 2.1: (a) Experimental system showing the molecular beam and TOF chambers connected by a skimmer, the MCP detector, and the pulsed valve on its XYZ translation stage. (b) Optical setup diagram. The Nd: YAG produces 532nm light to pump two dye lasers (SHG/THG). The fundamental beam of the dye lasers (750nm/606nm) is read by a wavemeter for monitoring. The main outputs (375nm/202nm) are combined and focused into the vacuum chamber.

2.2 Laser System

The second chamber has a window for laser access. We use dye lasers to get the wavelengths we want, where the gain medium is organic dyes used to produce coherent light. The main advantage of using dye lasers is tunability, as the output wavelength can be tuned over a wide range of the electromagnetic spectrum by changing dyes and adjusting optics[26]. Also, they have a relatively high power output. Currently, we are using the 2+1' scheme from Mackenzie et al.[1].

To produce wavelengths from Mackenzie et al.[1], we use SHG of ND:YAG pulse laser, which gives 5ns pulse at a rate of 10Hz. To produce 202nm for the excitation of N_2, we use the third harmonic generation (THG) of a dye laser (Lioptech, Liopstar, 3:1 Rhodamine 6G: DCM, in ethanol). To produce 375nm light for ionization, we use the second harmonic generation (SHG) of a dye laser (Lioptech, Liopstar, styryl 8, in ethanol). To minimize the ionization by 202nm, we use a polarizer and polarizing beam splitter (Figure 2.1b) to give a relatively lower output energy from the THG. 202nm and 375nm beams are focused in the second vacuum chamber.

Dye preparation:

- For 202nm:
    1. Take 1ltr ethanol in the reagent bottle (2000ml or any glass bottle for chemistry purposes).
    2. Put 0.045g of Rhodamine 6G and 0.15g of DCM.
    3. Fill up the ultrasonic bath with water such that after putting the bottle, the dye level is below the water level.
    4. Sonicate for 1hr.
    5. If the dye particles are still there, repeat the last step.
- For 375nm:
    1. Take 1ltr ethanol in the reagent bottle (2000ml or any glass bottle for chemistry purposes).
    2. Put 0.15g of Styryl 8 (LDS 751).
    3. Repeat 3-5 from above.

Note: Higher concentrations of dyes may damage the cell.

Changing dyes:

1. Empty all the dye from the circulators through the pipe below the dye bottles.
2. To wash out the remains of dye, put ethanol in dye bottles, circulate it for 2-3 minutes, and take it out.
3. Repeat step two, 3-4 times until all the dye gets out.
4. Now pour 900 ml from the prepared 1ltr dye solution for the Pre-amplifier dye bottle.
5. In the remaining 100ml, add 900ml of ethanol and sonicate for another hour.
6. Use this for the amplifier dye bottle.

Dye Maintainance:

- Periodic checking
    1. Monthly check the dye level in the dye bottle; if it is less than the mark, add ethanol until it reaches up to the mark.

2.3 Control hardware

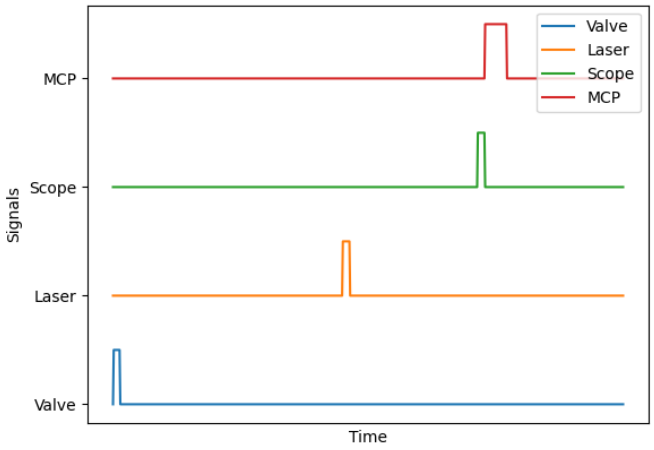

Figure 2.2: A TOF pulse sequence generated by the OPX+.(Not to scale)

The APV, pump laser, and MCP detection window are operated by Quantum Machines' OPX+, which also synchronizes other devices like shutters, power meters, wavemeters, etc. It is a programmable control hardware for 'synchronized multi-channel pulse sequences, pulse parametrization, real-time classical calculations, complex flow control with real-time decision-making, and ultra-low latency feedback' [27]. It can be operated using a Python script, and we can save the output data as a CSV file. We use OPX+ (see Figure 2.2 for our pulse scheme) to trigger the valve for 10μs; lasers are triggered after 315μs (the time it takes the molecular beam to reach the ionization region). The laser starts lasing, and the Pockel cell releases the beam and outputs a trigger voltage, which is then received by the OPX+. After receiving this trigger, the OPX+ triggers the Scope and the MCP simultaneously with no delay for taking measurements. MCP pulse width indicates a measurement window taking into account the time-of-flight of ions to the MCP. The reason behind taking input from Pockel's cell is there is a jitter of 3ns from actually triggering the laser and getting the output, which is then reduced to 1ns by this method.

Chapter 3

Results

3.1 REMPI

3.1.1 Time-of-flight of N_2^+

To get our first TOF signal, we set our 202nm laser at the Q-transition as it is the strongest transition (see Figure 3.3) and looked at the arrival times of ions using our TOF-MS. We observed a strong peak at 8.05μs (Figure 3.1), which we assigned to the $N_2{}^+$. To validate this, we moved the wavelength away from the resonance, which decreased the signal. Also, we increased the valve open time, delivering more N_2, which increased the signal. In Figure 3.1, the first peak at 0 is the signal from the laser, and the peak at 8.05 μs is the N_2^+ signal. For the small signal around 1.5 μs, we can use the mass dependence on TOF from Eq. 1.2,

$$m = \left(\frac{TOF_M}{TOF_{N_2}}\right)^2 * m_{N_2} = 0.972amu \tag{3.1}$$

According to this, we can assign this peak as a H^+ ion.

Apart from the mass and charge of an ion, the TOF signal depends on TOF-MS physical parameters such as the electrode distances (a, b, and c) and the applied voltages (V_{ext}, V_{rep}), see Figure 1.3. Also, the initial position where the ion is created (x) differs for each ion as they have a small spatial distribution in the ionization region. While we can accurately determine the voltages applied on the electrodes, the physical dimensions of the home-built TOF-MS are only estimated. Moreover, if we try to use the analytical derivation of section 1.4, these physical parameters become "effective" parameters. Lastly, the ionization position could deviate due to the misalignment of the laser. We performed a measurement to extract the "effective" physical parameters of our TOF-MS. We measured TOF

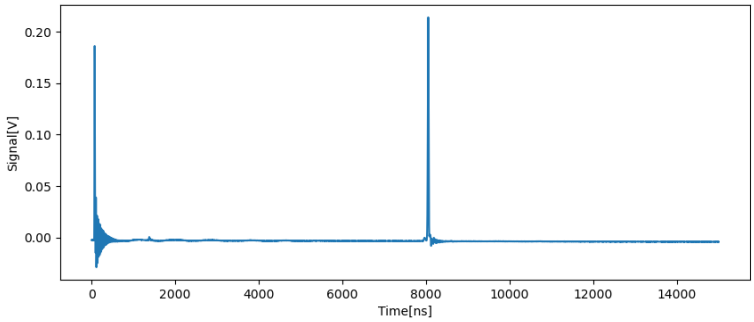

Figure 3.1: Signal on the MCP from N_2^+ ions created in the TOF-MS. The x-axis is the time-of-flight, and the y-axis is the signal in Volts.

values for different V_{ext} and V_{rep} voltages (see Figure 3.2). We globally fitted the experimental results to the analytical equation for the TOF (Eq. 1.8) with the physical parameters as fit parameters. The values are given in the caption of Figure 3.2. This calibration measurement can interpolate and extrapolate the TOF for different TOF voltages.

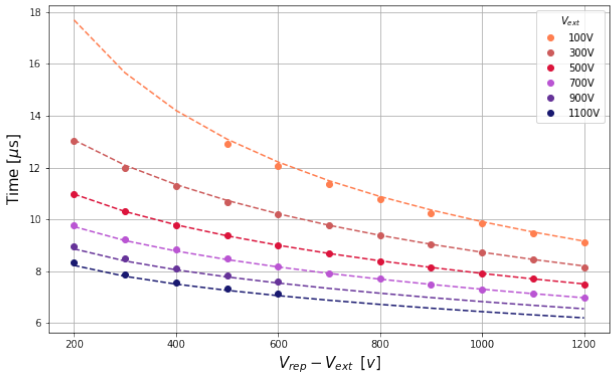

Figure 3.2: TOF values for different V_{ext} and V_{rep} voltages. Dashed lines are the results of a global fit to the analytical TOF equation 1.8. The best fitting parameters for our system we found are $a = 3.75cm, b = 0.8cm, c = 60.05cm$.

As we mentioned earlier, the ions formed have a spatial distribution; as they reach the extractor electrode, they will have a large spatial distribution. This spread depends on the initial velocity before the acceleration of the ion[28]. To counteract this delay, we can choose the delay between the repeller electrode and the extractor by changing V_{ext} and V_{rep} values such that ions of a particular m/z

will focus sharply at the detector plane. We have all the parameters we need from the simulation we ran for Figure 3.2. Optimizing values of V_{ext} and V_{rep}, using these parameters, will help us to have a minimal dispersion in the time-of-flight despite the initial position of the ion for the given m/z.

3.1.2 2+1 REMPI spectrum

We performed the scan of 202nm laser to get the REMPI spectrum of N_2, which reveals the transition between the electronic ground state to the electronic-intermediate state. We blocked the 375nm laser during this process. Figure 3.1 shows the signal from TOF-MS for one measurement. While scanning, we took multiple measurements for a single wavelength. As the number of ionized molecules is proportional to the intensity of the signal, we had two options to analyze the data in Figure 3.1: extracting the maximum peak or calculating the area under the curve. We tried both methods to see which one is the better. In the S(0) transition region, the area method is better than the maximum method by ~10% (comparisons have been made based on standard deviation). Thus, since both methods give roughly the same results, we used the maximum, which is a more straightforward method to implement.

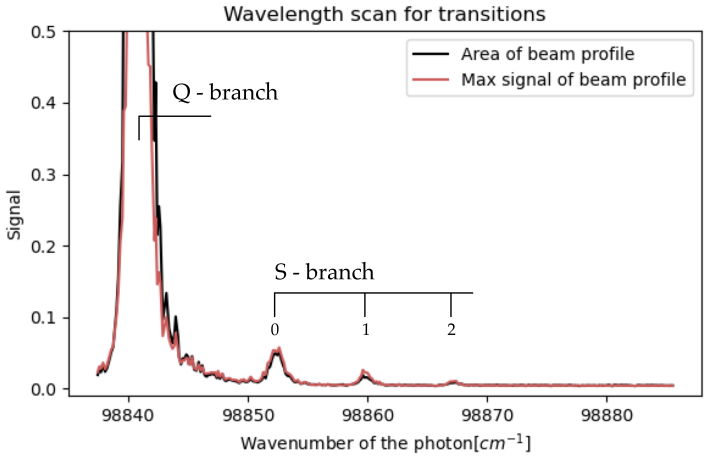

Figure 3.3: MCP signal as a function of the 202nm laser wavenumber showing resonances in the N_2 spectrum. Black and red curves are two different methods to analyze the MCP signal (see text for details).

Our REMPI spectrum results match with Mackenzie et al.[1]. In Figure 3.3, the most prominent peak belongs to the Q(J) transition; electrons jump from the lower electronic state to the higher electronic state without changing the rotational state

($\Delta J = 0$). Other peaks represent the S transition where the rotational state of the higher electronic state is higher by two than the lower electronic state ($\Delta J = +2$). For S-transitions, we know the initial and final rotational state, but in the case of Q(J), resolving the rotational state is not possible due to the linewidth of our laser. Hence, it is not state-selective. As the S(0) transition is the most dominant from the state-selective transitions, we will use it for the 2+1' REMPI scheme.

We took the REMPI spectrum at different valve open timings; the result is represented in Figure 3.4. We can see that for opening times longer than 54μs, and the is almost the same. This happens due to the saturation of N_2 molecules, i.e., on increasing the valve open time, N_2 density remains constant after one point.

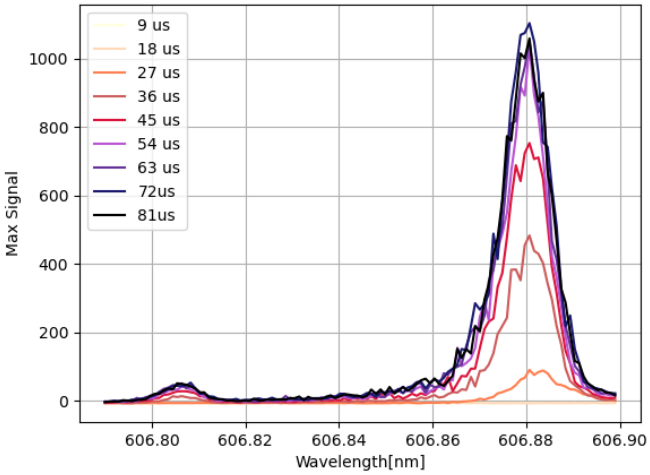

Figure 3.4: The effect of valve open time on the REMPI spectrum. The big peak is the Q(J) transition, while the small peak is the S(0) transition. Wavelength is that of the THG dye laser fundamental.

3.1.3 2+1' REMPI

To observe the 2+1' REMPI scheme from Mackenzie et al.[1], we proceeded with the 54μs valve open time and set the first photon to the wavelength where we get the S(0) transition and use low enough power to excite the N_2, which helps us put restrictions on ionizing the molecule. We scanned the 375nm laser to look for a step-like function in the intensity of the signal after passing the ionization threshold (see Figure 3.5). As in REMPI, for the second transition to make N_2^+, the electron moves from one Rydberg state to another. The ionization channel opens as the molecule gets high enough energy. We observe the 2+1' signal at a low steady state,

starting to increase after 125625 cm^{-1} and reaching a higher steady state. Whereas 2+1 is constant throughout the measurement. Below the ionization threshold, the 2+1' signal is lower than the 2+1 signal, indicating inhibition of 202nm photons by 375 nm photons. We scanned 330 wavenumbers, repeating the measurement ten times for each wavenumber. For N_2^+, the vibrational and rotational ground state term value is $\sim$ 125666 cm^{-1} [1]. The shift we see here from theoretical value is most likely due to the presence of the DC electric field in the ionization region. Thus, we plan to use a fast HV switch to switch on the fields just after the ionization.

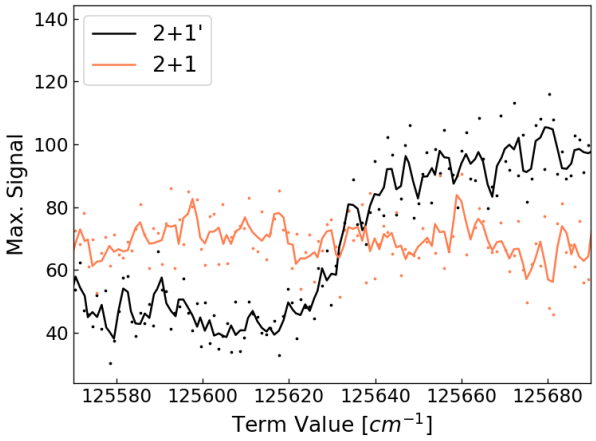

Figure 3.5: State-selective ionization of N_2. The spectrum of 2+1' (black) and 2+1 (orange) schemes. While measuring the 2+1 scheme, the 375nm laser was mechanically blocked. Scattered points are actual data, and a solid line represents the moving average of actual data.

3.2 HV Switch

3.2.1 Testing of the switch

We are using GHTS60 High Voltage push-pull switch from BEHLKE. The switch is triggered using OPX+ at 10 Hz. The output of the OPX+ is 1.1V at high impedance. However, the trigger input for the HV switch must be at least 2V(at max 5V) with low impedance. Thus we have to build a circuit that converts low voltage from the OPX+ to high voltage while changing the impedance to low.

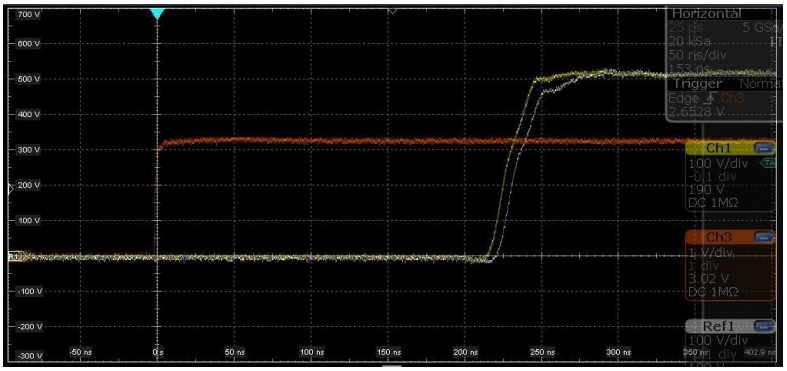

Figure 3.6: Measurement of the switch delay. Red is the trigger, and yellow and white are the output from two HV switches.

The input voltage is given with the high-voltage power supply. To check the delay between the trigger and the output from the switch, an N2891A 70MHz Differential probe by KEYSIGHT at 1000:1 attenuation was used. The switch was checked for the triggers with various frequencies. We observed a delay of 228.66 ± 0.28 ns with a rise time of 23.38 ± 0.32 ns for one switch and a delay of 234.57 ± 0.62 ns with a rise time 27.06 ± 0.12 ns for the other. The ion takes $6\mu s$ to leave the ionization region, so even with the delay of 230ns, we get sufficient time to turn on the electric field for spectroscopic measurements.

3.2.2 Assembly

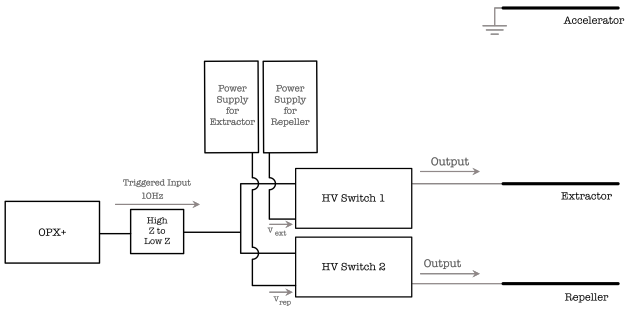

Figure 3.7: Schematic of high-voltage switch implementation.

We plan to keep both the repeller and the extractor electrode at 0V. We have to use 2 switches, one for the repeller and the other for the extractor, as the switch has a single input and output. After making all the connections shown in figure 3.7, the first step would be to perform a measurement to scan the delay between the ionization and switching the electrodes, and selecting the delay will make sure that the electric field does not affect the ionization while preventing ion loss.

3.3 Calcium oven

3.3.1 Design

Currently, ions are loading to the ion trap using an oven located near the ion trap (in the future, the ion trap will be connected to the molecular beam setup after the TOF chamber). Here, we are experimenting with a new way to load ions using the molecular beam. A new home-built oven is designed in such a way that it will spray calcium atoms, which a molecular beam will further carry to the trap. The oven will be located in the valve chamber, $\sim$1 meter away from the ion trap. The red part (oven) in Figure 3.8a is a 316L stainless steel very thin tube that contains solid calcium, our source. We chose stainless steel due to its high electrical resistivity, 74 $\mu\Omega$·cm. The oven and electrical connections are separated by 316L stainless steel thick connectors (green part in Figure 3.8a) with low thermal conductivity (14.0 - 15.9 W/m·K) to avoid excessive heating of the electric circuit (copper wires).

We mounted the calcium oven in front of the APV in the first chamber, which delivers the N_2 into the system. However, there is a possibility of excess calcium blocking the opening of the valve. Also, we don't want our vacuum system to get filled up with unnecessary calcium as that might harm other system parts, e.g., the skimmer and turbo pump. Thus, we built a chamber around our oven (yellow) made up of stainless steel. This chamber has two holes, the smaller one for N_2 beam to enter and another for the exit of N_2 along with Ca. We use ceramic material (Blue) to avoid the current flow to the chamber and hold the oven. To adjust the distance of the oven from the N_2 beam, we have small rods (brown) on which the chamber can slide.

3.3.2 Cleaning

For cleaning the homemade Ca oven, we used Deconex 36-Intensive with a neutral pH and mixed it with the deionized water at a ratio of 1:100. We put the parts in an ultrasonic bath for half an hour, then washed them again with the deionized

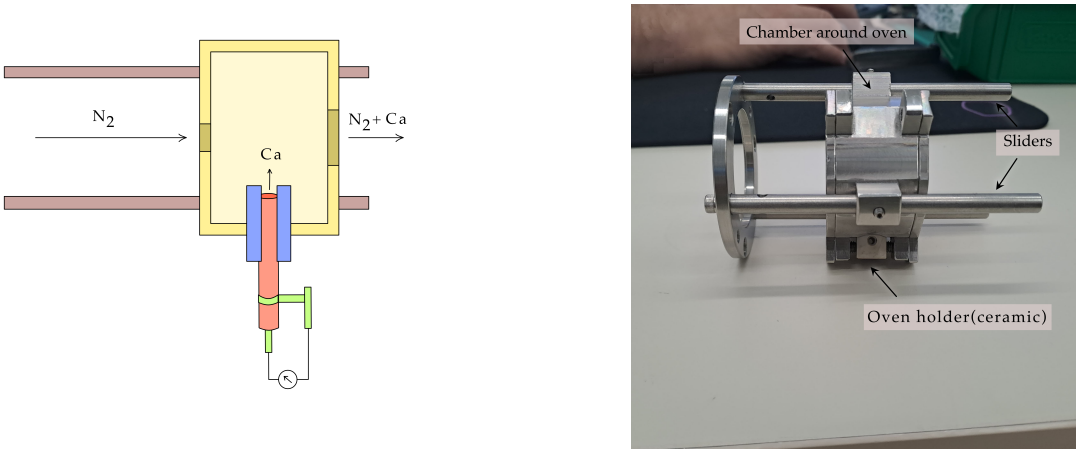

(a) (b)

Figure 3.8: a) Schematic of the Home-built oven design. b) Picture of the part that we have manufactured in-house.

water only for another half an hour. After that, we thoroughly cleaned the part with a stream of deionized water to get rid of residual dirt or leftover detergent.

3.3.3 Testing of the oven

We built a small vacuum setup to check the calcium oven. The pressure of the vacuum system was maintained at 10^{-7} mbar. After turning on the oven, the pressure increased to 10^{-4} mbar due to the heating of the oven, and it took around half an hour to go back to the 10^{-7} mbar. To observe the vaporized calcium, the calcium was excited from $^1S_0$ state to $^1P_1$ state using 422nm laser, which gives atomic fluorescence[29]. The current was set to 10A to heat the oven, and the wavelength was scanned from 420nm to 424nm. We observed the fluorescence at 422.791784(22)nm.

3.3.4 Preliminary searches for Ca^+ TOF-MS signal

After installing the Ca oven in front of the APV valve, we used the molecular beam to carry the calcium to the ionization chamber, where the 202nm laser ionizes both the Ca and N_2. As TOF-MS has a mass resolution of 250 and more, we can use it to detect the Ca ion. We expect to see two peaks in the signal on the MCP. As we know, mass depends on the square of the time traveled (Eq. 1.2). Our TOF-MS is already calibrated by the N_2 peak at 8.05μs, so we expect to find a

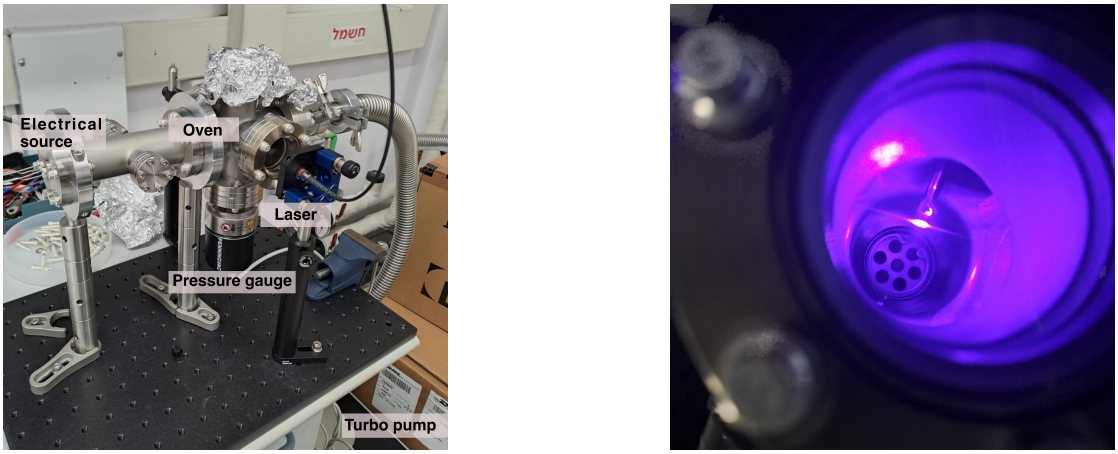

(a) Vacuum setup (b) Calcium Fluorescence

Figure 3.9: Testing the calcium oven using laser fluorescence.

signal that belongs to Ca^+ by using the relation given in the Eq. 3.2. We hope to see the Ca^+ peak at 9.62μs.

$$TOF_{Ca} = \left(\sqrt{\frac{m_{Ca}}{m_{N_2}}}\right) * TOF_{N_2} = 9.62\mu s \tag{3.2}$$

First, we had to check if the N_2 beam was the same without the Ca oven. Our aperture for the molecular beam to enter the oven can affect the beam properties. We observe the reduction in the N_2^+ signal. For effective selective ionization, the ground state population should be maximum; this means the molecular should be sufficiently cold. However, the oven is in the way of the molecular beam, and the molecules hit the walls of the oven, causing an increase in the temperature of molecules. In Figure 3.10, we see multiple peaks in the hot spectrum (measurements taken with the oven) and with the 2:1 alternating intensity pattern. From this, it is evident that the molecular beam is hot. Furthermore, for our experiment, we need S(0) transition. However, from Figure 3.10, we can see the S(0) peak is submerged in the Q(J) peak. Thus, we have decided instead of having a small aperture for N_2 to pass to keep open the sides facing the valve and to the skimmer. We still need to verify that this will reduce the molecular collisions and hence retrieve the molecular beam to its colder state.

Furthermore, we tried to look for the Ca signal. However, with no success yet. In the last few weeks of my project, I worked to increase the 375nm laser power

to its original state (5mJ at full power of ND:YAG). With this increased power, we expect to have a better chance of observing the Ca signal on the TOF-MS.

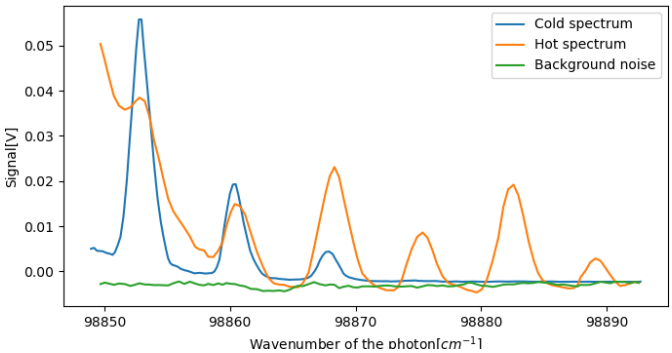

Figure 3.10: 2+1 REMPI spectrum. Blue is the measurements without the oven, Orange is with the oven, and Green is the background noise.

Chapter 4

Dual Frequency

Due to the unexpected start of hostilities in Israel, we found a bit of a plot twist, a swift change of scenery back home. In the absence of being in a lab, we started working on an important computational project that will help us in our future endeavors. Whether under the glow of lab lights or the glow of our computer screens, science must go on!

4.1 Generic paul trap

There are different methods to trap an ion, such as Penning traps, multipole traps, and optical dipole traps. The workhorse for quantum-information applications is definitely the Paul trap, and this is the type of trap we are using in our lab. This project explores the capability of the Paul trap to confine two atomic ions with significantly distinct masses, e.g., the Ca^+ and I_2^+ atomic and molecular ions with masses of 40u and 254u, respectively. The conventional traps use the single-frequency trapping method, which fails at such disparate mass ions (typically, masses up to ∼X3 are stable in the same trap). We would like to investigate a dual-frequency Paul trap to maintain stable trapping conditions for the ions with a large mass difference. This work is inspired by the work of Trypogeorgos et al.[30], which considered the confinement of two ions with extremely different masses (e.g., an atomic ion and a nano-particle). Here, we try to test the feasibility of this work to more moderate mass differences.

In a symmetric linear Paul trap shown in 4.1, GND (blue) and DC (green) electrodes are kept at rf-ground whereas rf voltage (V_{RF}) is applied at frequency Ω on the RF (red) electrode. Electric potential is quadratic in the region close to the trap center and only has a radial component,

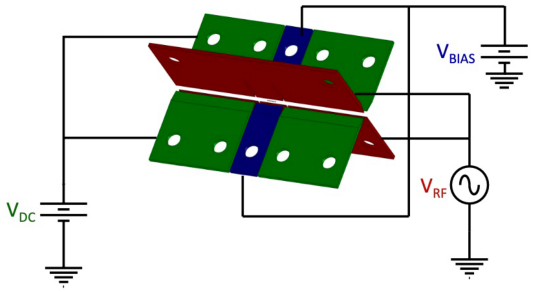

Figure 4.1: Schematic of trap electrode design. Taken from [31].

$$\mathrm{V}(x,y,t) = \frac{\mathrm{V_{RF}}}{2}\left(1+\frac{x^2-y^2}{R_0'^2}\right)\cos(\Omega t). \tag{4.1}$$

Here, R_0 is the center-of-trap to electrode distance and $R_0' = \epsilon_{R_0'} R_0$, where $\epsilon_{R_0'}$ is a geometrical factor (for hyperbolic electrodes $\epsilon_{R_0'} = 1$). Degeneracy of the ion's radial modes arises due to the cylindrical symmetry of a radial potential (Eq. 4.1). A dc voltage ($\mathrm{V_{BIAS}}$) on the GND (blue) electrode removes this degeneracy,

$$\mathrm{U}_1(x,y,t) = \frac{\mathrm{V_{BIAS}}}{2}\left(1+\frac{x^2-y^2}{R_0'^2}\right), \tag{4.2}$$

In linear Paul traps, radial trapping is done by the rf electric fields while the axial (z-direction) trapping is carried by a constant (dc) voltage ($\mathrm{V_{DC}}$) that is applied on the DC electrodes (green). The static potential near the trap center created is,

$$\mathrm{U}_0(x,y,z,t) = \frac{\mathrm{V_{DC}}}{Z_0'^2}\left[z^2-\frac{1}{2}\left(x^2+y^2\right)\right]. \tag{4.3}$$

Here, $Z_0' = \epsilon_{Z_0'} Z_0$, is the effective center-of-trap-electrode distance. From these rf and dc electric potentials, we get the classical equations of motion for an ion with mass m and charge e in the form of a Mathieu equation [32],

$$\ddot{u}_i + u_i\left[a_i + 2q_i\cos(\Omega t)\right]\frac{\Omega^2}{4} = 0, \tag{4.4}$$

Where u_i is the displacement of the ion from the trap center along axis $i = x, y, z$. Whereas, a_i and q_i are trap parameters given by,

$$\begin{aligned} a_{x/y} &= -\frac{4e}{m\Omega^2}\left(\frac{\mathrm{V_{DC}}}{Z_0'^2} \mp \frac{\mathrm{V_{BIAS}}}{R_0'^2}\right), \quad a_z = \frac{8e}{m\Omega^2}\frac{\mathrm{V_{DC}}}{Z_0'^2} \\ q_x &= -q_y = \frac{2eV_r f}{mR_0'^2\Omega^2}, \quad q_z = 0. \end{aligned} \tag{4.5}$$

The analytical approximate solution (second order) looks like [33],

$$u_i \approx A_i \left(\cos\left(\omega_i t + \phi_i\right)\left[1 + \frac{q_i}{2}\cos(\Omega t) + \frac{q_i^2}{32}\cos(2\Omega t)\right] + \frac{\omega_i}{\Omega} q_i \sin\left(\omega_i t + \phi_i\right)\sin(\Omega t)\right). \tag{4.6}$$

Most often, we use the first-order analytic approximation,

$$u_i \approx A_i \cos\left(\omega_i t + \phi_i\right)\left[1 + \frac{q_i}{2}\cos(\Omega t)\right]. \tag{4.7}$$

The ion's motion is described by the secular motion with the frequency $\omega_i \approx \frac{\Omega}{2}\sqrt{a_i + q_i^2/2}$, amplitude A_i and with the phase ϕ_i and the micromotion part with frequency $\Omega \pm \omega_i$ with an amplitude $\frac{A_i q_i}{2}$(see figure 4.3).

We used Python's 'odeint' solver (see Appendix A) to find the motion of a single trapped ion and compared it with the second-order analytical approximation.

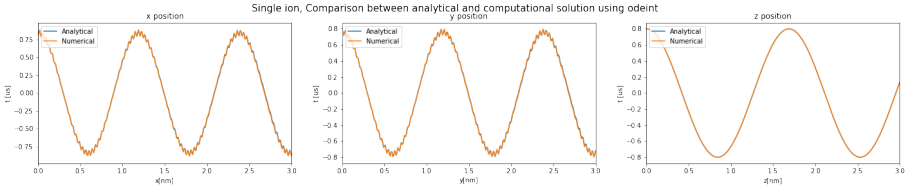

Figure 4.2: Motion of a single ion trapped in a Paul trap with the parameters, $a_x = a_y = -0.001, a_z = 0.001, q_x = -0.1, q_y = 0.1$. The orange line is the numerical integration of Eq. 4.4 while the blue line is the analytical approximation of Eq. 4.6.

We see that in a linear Paul trap confinement of the ion in the radial axes($i = x, y$), the energy is distributed between secular motion and micromotion; as both of them are kinetic, the total energy is purely kinetic. Furthermore, the confinement

in the z-axis is purely harmonic, with an equal distribution of kinetic and potential energy. The total kinetic energy in along each axis is $E_i = \frac{1}{2}(A_i\omega_i)^2$ with an amplitude of A_i. From figure 4.3, it is evident that secular and micromotion frequencies calculated using numerical methods match analytical calculations.

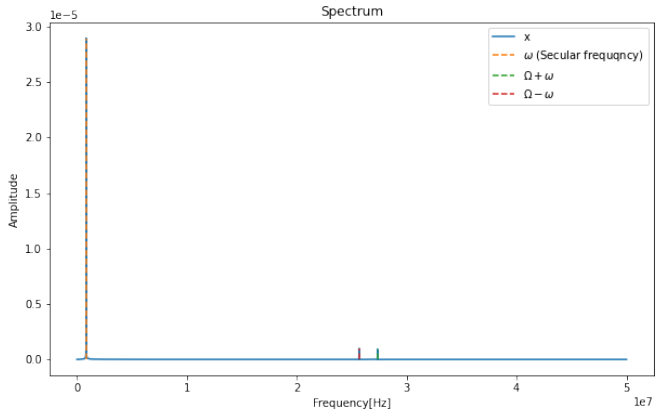

Figure 4.3: The blue line is the Fourier transform of the motion of a single ion trapped in a Paul trap derived by numerically integrating Eq. 4.4 ω is the secular frequency and $\Omega \pm \omega$ is the micromotion frequency.

We now continue to solve the dynamics of two ions trapped in a single-frequency Paul trap(see Appendix A). Since the two ions are charged, they will experience a Coulomb force, and their equations of motion will look like this,

$$\ddot{u}_{i,j} + u_{i,j}\left[a_{i,j} + 2q_{i,j}\cos(\Omega t)\right]\frac{\Omega^2}{4} + \frac{e^2}{4\pi\varepsilon_0 m_j}\frac{u_j - u_{j'}}{r_{ab}^3} = 0. \tag{4.8}$$

Here, j is an index of ion 'a' or ion 'b' for which we calculate the dynamics, and $j^{'}$ is the index of the other ion, r_{ab} is the distance between two ions, m_j is the mass and ε_0 is the vacuum permittivity. This will give us 6 equations of motion, 3 for each ion. The simulation of the motion of two ions by slightly disturbing them in one direction is shown in Figure 4.4. There are mainly 4 cases:

- **Same masses**

  When two ions with identical masses are displaced in the same direction by the same distance (here, $1\,nm$), they exhibit in-phase motion with the same frequency at the same amplitude. In the radial direction($i = x, y$),

the energy is distributed in secular and micromotion. The frequency of the secular motion is[1], $\omega_{-,i} = \frac{\Omega}{2}\sqrt{\frac{q_i^2}{2} + a_i}$, as for $m_1 = m_2$, $q_{i,1} = q_{i,2} \equiv q_i$ and $a_{i,1} = a_{i,2} \equiv a_i$. The frequency of a micromotion is $\omega_i \pm \Omega$. In the axial direction, both ions perform harmonic motion with frequency[1] $\omega_{-,z} = \frac{\Omega}{2}\sqrt{a_z}$ as $q_z = 0$.

When two identical masses are displaced in opposite directions by the same distance (here, $1\,nm$), it exhibits out-of-phase modes in all axes. The secular motion has a frequency[1], $\omega_{+,i} = \frac{\Omega}{2}\sqrt{\frac{q_i^2}{2} + 3a_i}$ as for same masses $q_{i,1} = q_{i,2} \equiv q_i$ and $a_{i,1} = a_{i,2} \equiv a_i$. The frequency of a micromotion in the radial axis will be $\omega_i \pm \Omega$. In the axial direction, both ions perform harmonic motion with frequency[1] $\omega_{+,z} = \frac{\Omega}{2}\sqrt{3a_z}$ as $q_z = 0$.

In the problem of ions with two equal masses, we have two frequencies, ω_+ corresponding to out-of-phase mode, and ω_- corresponding to in-phase mode. These modes correspond to the stretched and center-of-mass modes of the ions, respectively.

- **Different masses**

When two ions with different masses are displaced, they oscillate with the frequency[1],

$$\omega_{i,\pm} = \Omega\sqrt{\frac{q_{i,1}^2 + q_{i,2}^2 + 4a_{i,1}(1+\mu) + \sqrt{((q_{i,1}^2 + 4a_{i,1}) - (q_{i,2}^2 + 4a_{i,2}))^2 + (4a_{i,1})^2\mu}}{16}}. \tag{4.9}$$

in the radial direction ($i = x,\ y$). Where, $\omega_{i,+}$ is out-of-phase frequency and ω_- is in-phase frequency. And $\mu = \frac{m_1}{m_2}$. Whereas in the axial direction,

$$\omega_{z,\pm} = \frac{u_0}{m}\left(1 + \mu \pm \sqrt{1 + \mu^2 - \mu}\right). \tag{4.10}$$

Where, $u_0 = \frac{eV_{DC}}{Z_0^2}$When $\mu > 1$ (In our case $\mu = 1.428$). However, in the case of different masses, these two modes are not separable. In this case, these two modes are coupled and not related to COM anymore.

[1]Frequency calculations are done by Dror Einav, master's student in our group

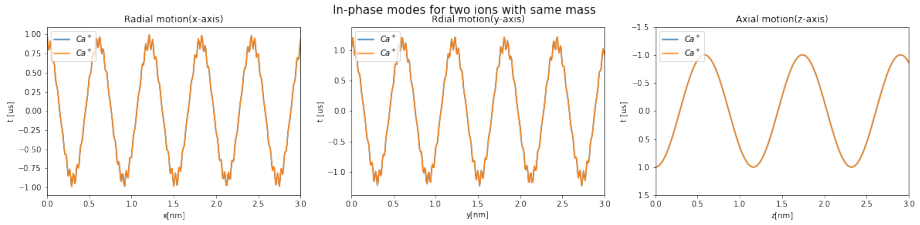

(a) Two ions with the same mass (40amu, Ca^+ ions) disturb from their equilibrium position in the same direction by 1 nm.

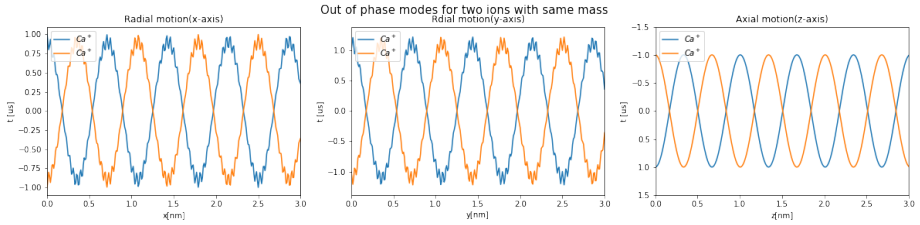

(b) Two ions with the same mass (40amu, Ca^+ ions) disturb from their equilibrium position in the opposite direction by 1 nm.

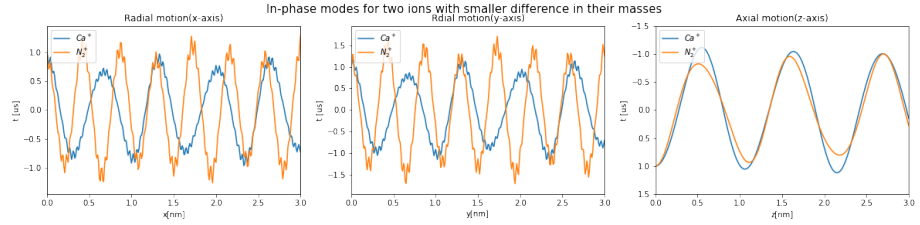

(c) Two ions with different masses (Ca^+ and N_2^+ ions, 40amu, and 28amu respectively) disturb from their equilibrium position in the same direction by 1 nm.

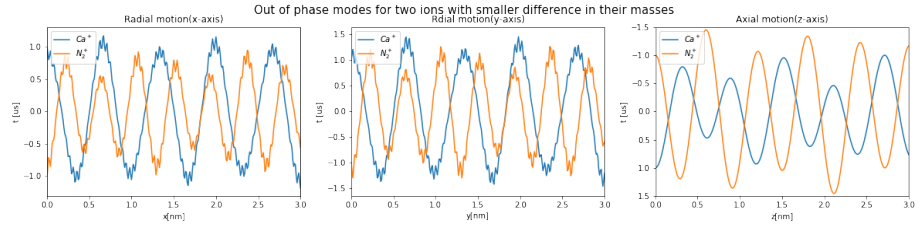

(d) Two ions with different masses (Ca^+ and N_2^+ ions, 40amu, and 28amu respectively) disturb from their equilibrium position in the opposite direction by 1 nm.

Figure 4.4: Motion of two ions trapped in a Paul trap, this calculation is done with parameters, $\Omega = 24MHz, R_0' = 0.716mm, Z_0' = 9.04mm, V_{DC} = 500V, V_{rf} = 500V$, these parameters are taken from [31]

4.2 Dual-frequency Paul trap

We want to investigate the possibility of the dual-frequency trap to maintain stable conditions for trapping two ions with larger mass differences. For the dual-frequency trap, Eq. 4.1 will become,

$$\mathrm{V}(x,y,t) = \frac{1}{2}\left[V_{rf_1}\cos(\Omega_1 t) + V_{rf_2}\cos(\Omega_2 t + \phi)\right]\left(1 + \frac{x^2 - y^2}{R_0'^2}\right). \tag{4.11}$$

Where there are two RF voltages V_{rf_1} and V_{rf_2} applied at frequency Ω_1 and Ω_2. This will result in the equation of motion of an ion trapped in a dual-frequency trap,

$$\ddot{u}_i + u_i\left[a_i\frac{\Omega_1^2}{4} + 2q_{1i}\frac{\Omega_1^2}{4}\cos(\Omega_1 t) + 2q_{2i}\frac{\Omega_2^2}{4}\cos(\Omega_2 t)\right] = 0, \tag{4.12}$$

$$\begin{aligned} a_{x/y} &= -\frac{-4e}{m_1\Omega_1^2}\left(\frac{\mathrm{V_{DC}}}{Z_0'^2} \mp \frac{\mathrm{V_{BIAS}}}{R_0'^2}\right), \quad a_z = \frac{8e}{m_1\Omega_1^2}\frac{\mathrm{V_{DC}}}{Z_0'^2} \\ q_{1x} &= -q_{1y} = \frac{-2eV_{rf_1}}{m_1 R_0'^2\Omega_1^2}, \quad q_{1z} = 0, \\ q_{2x} &= -q_{2y} = \frac{-2eV_{rf_2}}{m_2 R_0'^2\Omega_2^2}, \quad q_{2z} = 0. \end{aligned} \tag{4.13}$$

Thus for two ions trapped in a trap, the equation of motion will be,

$$\ddot{u}_{i,j} + u_{i,j}\left[a_{i,j}\frac{\Omega_1^2}{4} + 2q_{1i,j}\frac{\Omega_1^2}{4}\cos(\Omega_1 t) + 2q_{2i,j}\frac{\Omega_2^2}{4}\cos(\Omega_2 t)\right] + \frac{e^2}{4\pi\varepsilon_0 m_j}\frac{u_j - u_{j'}}{r_{ab}^3} = 0. \tag{4.14}$$

To check if this is correct, we did a simulation for Ca^+ and N_2^+ ion(see Appendix A) with $\Omega_1 = \Omega_2$ and $V_{rf_1} = V_{rf_2}$, and results matched with figure 4.4. Now we have to scan the Ω_2 and corresponding V_{rf_2} to find the stable parameters.

Chapter 5

Discussion

We performed the simulation to find the best conditions to improve the precision of the time of flight. It corroborates the refined nature of ion manipulation in the TOF-MS. We can enhance the ion focusing by carefully choosing the V_{ext} and V_{rep}. It mitigates the effect of the spatial distribution and maximizes the precision of mass spectrometry.

We have also performed measurements for single-photon ionization (2+1 REMPI) using 202nm while 375nm was blocked. We observed the 2+1 REMPI spectrum of the N_2, and from there, we got the S(0) wavelength, which we require for our further expedition. We also calibrated the valve opening timings and found the peak intensity stabilizes for 54 μs due to the nitrogen saturation. Further, we performed a 2+1' REMPI spectrum by reducing the power of the S(0) transition to avoid non-selective transition. We observed a step-like function when a 375 nm laser passed the ionization threshold. We see that 2+1' ionization starts at the value 125625 cm^{-1}, possibly due to the DC extraction field, as the electric fields, which extract the molecular ions into a detector, are constantly present in the ionization region. This also leads to a reduction in the state selectivity of ionization due to an inhomogeneous electric field environment. Detailed measurements for the effect of the DC extraction field on ionization energy can be found in Idan Hochner's master's thesis and Mackenzie et al.[1]. We plan to implement the high-voltage switch into the existing system to mitigate the electric fields during the ionization pulse and characterize the effect of the voltage switching on the ionization state selectivity. The preliminary tests of switches show that the delay and the rise time in the switch's response are acceptable. We plan to keep the repeler and extractor electrodes on 0V and then activate the electric field post-ionization. Also, as discussed in section 3.1, we plan to switch the REMPI wavelengths explained in Gardener et al.[21] to get much better state selectivity. We will characterize this scheme compared to the old one.

The novel oven design we have implemented promises to load Calcium will help us to load Calcium ions using the molecular beam. This promises to enhance the ion trapping efficiency. The homemade oven is designed so that its distance from the valve is adjustable. Also, it will help us mitigate the unnecessary accumulation of Calcium in the system. We observed the fluorescence by Calcium, confirming the working of the oven. However, we observed a decrease in the N_2^+ signal as well as with the oven in the way the molecular beam is not sufficiently cold. We need to upgrade the design so that molecular collisions with the oven will be reduced, thereby preserving the ground state population. This will help us enhance the S(0) transition of the Nitrogen. We also need to increase the power output of the 375nm laser, as the current output is less than the optimal required for efficient ionization. By accomplishing this, we desire to improve the ion-loading process.

In our theoretical project, we aim to tackle the possibility of a Dual-frequency Paul trap to achieve stable conditions for confining two ions with substantial mass discrepancies. Preliminary results confirm the accuracy of our theoretical model for the Dual-frequency Paul trap when we use equal frequencies and rf voltage for Ca^+ and N_2^+. The subsequent step will be, scanning the values of Ω_2 and V_{rf_2} to find the necessary stable conditions. This exploration will help us advance the operational scope of the Paul trap by presenting the significant advancement in precision ion trapping.

Though the journey ahead is extensive, this project lays the groundwork for the new pathways for future investigations to enhance the field of the quantum control of complex molecules and precision ion-trapping.

Bibliography

[1] S. Mackenzie, F. Merkt, E. Halse, and T. P. Softley, "Rotational state selectivity in n_2^+ $x^2\Sigma_g^+(\nu+=0)$ by delayed pulsed field ionization spectroscopy via the $a^1\Sigma_g^+(\nu=0)$ state", Molecular Physics **86**, 1283–1297 (1995).

[2] S. Haroche, "Nobel lecture: controlling photons in a box and exploring the quantum to classical boundary", Rev. Mod. Phys. **85**, 1083–1102 (2013).

[3] H. Margolis, "Optical frequency standards and clocks", Contemporary Physics **51**, 37–58 (2010).

[4] M. Sinhal, Z. Meir, K. Najafian, G. Hegi, and S. Willitsch, "Quantum-nondemolition state detection and spectroscopy of single trapped molecules", Science **367**, 1213–1218 (2020).

[5] F. Wolf, Y. Wan, J. C. Heip, F. Gebert, C. Shi, and P. O. Schmidt, "Quantum logic with molecular ions", arXiv preprint arXiv:1507.07511 (2015).

[6] C.-w. Chou, C. Kurz, D. B. Hume, P. N. Plessow, D. R. Leibrandt, and D. Leibfried, "Preparation and coherent manipulation of pure quantum states of a single molecular ion", Nature **545**, 203–207 (2017).

[7] Y. Lin, D. R. Leibrandt, D. Leibfried, and C.-w. Chou, "Quantum entanglement between an atom and a molecule", Nature **581**, 273–277 (2020).

[8] S. Patra, M. Germann, J.-P. Karr, M. Haidar, L. Hilico, V. Korobov, F. Cozijn, K. Eikema, W. Ubachs, and J. Koelemeij, "Proton-electron mass ratio from laser spectroscopy of hd+ at the part-per-trillion level", Science **369**, 1238–1241 (2020).

[9] K. Najafian, Z. Meir, and S. Willitsch, "From megahertz to terahertz qubits encoded in molecular ions: theoretical analysis of dipole-forbidden spectroscopic transitions in n 2+", Physical Chemistry Chemical Physics **22**, 23083–23098 (2020).

[10] A. Kruckenhauser et al., "Quantum many-body physics with ultracold polar molecules: nanostructured potential barriers and interactions", Phys. Rev. A **102**, 023320 (2020).

[11] F. Diedrich, J. Bergquist, W. M. Itano, and D. Wineland, "Laser cooling to the zero-point energy of motion", Physical review letters **62**, 403 (1989).

[12] K. Mølhave and M. Drewsen, "Formation of translationally cold MgH^+ and MgD^+ molecules in an ion trap", Phys. Rev. A **62**, 011401 (2000).

[13] X. Tong, A. H. Winney, and S. Willitsch, "Sympathetic cooling of molecular ions in selected rotational and vibrational states produced by threshold photoionization", Physical review letters **105**, 143001 (2010).

[14] A. Hansen, O. Versolato, Ł. Kłosowski, S. Kristensen, A. Gingell, M. Schwarz, A. Windberger, J. Ullrich, J. C. López-Urrutia, and M. Drewsen, "Efficient rotational cooling of coulomb-crystallized molecular ions by a helium buffer gas", Nature **508**, 76–79 (2014).

[15] S. A. Moses, J. P. Covey, M. T. Miecnikowski, D. S. Jin, and J. Ye, "New frontiers for quantum gases of polar molecules", Nature Physics **13**, 13–20 (2017).

[16] L. R. Liu, J. D. Hood, Y. Yu, J. T. Zhang, N. R. Hutzler, T. Rosenband, and K.-K. Ni, "Building one molecule from a reservoir of two atoms", Science **360**, 900–903 (2018), eprint: `https://www.science.org/doi/pdf/10.1126/science.aar7797`.

[17] G. M. Tino, "Identical particles exchange symmetry and the electric dipole moment in molecules", Symmetry **14**, 2397 (2022).

[18] M. Germann, "Dipole-forbidden vibrational transitions in molecular ions a novel route to precision spectroscopy and studying effects of interest to fundamental physics", PhD thesis (2016).

[19] A. Kantrowitz and J. Grey, "A high intensity source for the molecular beam. part i. theoretical", Review of Scientific Instruments **22**, 328–332 (1951).

[20] U. Boesl and R. Zimmermann, "Fundamentals and mechanisms of resonance-enhanced multiphoton ionization (rempi) in vacuum and its application in molecular spectroscopy", Photoionization and Photo-Induced Processes in Mass Spectrometry: Fundamentals and Applications, 23–88 (2021).

[21] A. Gardner, T. Softley, and M. Keller, "Multi-photon ionisation spectroscopy for rotational state preparation of n 2+", Scientific Reports **9**, 506 (2019).

[22] M. Wolff and W. Stephens, "A pulsed mass spectrometer with time dispersion", Review of Scientific Instruments **24**, 616–617 (1953).

[23] W. Wiley, "Time-of-flight mass spectrometer with improved resolution", Review of scientific instruments **26**, 1150–1157 (1955).

[24] B. Mamyrin, V. Karataev, D. Shmikk, and V. Zagulin, "The mass-reflectron. a new nonmagnetic time-of-flight high resolution mass-spectrometer", Zhurnal Ehksperimental'noj i Teoreticheskoj Fiziki **64**, 82–89 (1973).

[25] W. Wiley and I. H. McLaren, "Time-of-flight mass spectrometer with improved resolution", Review of scientific instruments **26**, 1150–1157 (1955).

[26] H. J. Eichler, J. Eichler, O. Lux, H. J. Eichler, J. Eichler, and O. Lux, "Dye lasers", Lasers: Basics, Advances and Applications, 121–130 (2018).

[27] Q. M. OPX+, `https://qm-docs.qualang.io/introduction/qop_overview.`, [Accessed 03-12-2023].

[28] M. Guilhaus, "Special feature: tutorial. principles and instrumentation in time-of-flight mass spectrometry. physical and instrumental concepts", Journal of mass spectrometry **30**, 1519–1532 (1995).

[29] N. Beverini, E. Maccioni, F. Sorrentino, V. Baraulia, and M. Coca, "Measurementof the transition probability in calcium", The European Physical Journal D-Atomic, Molecular, Optical and Plasma Physics **23**, 223–228 (2003).

[30] D. Trypogeorgos and C. J. Foot, "Cotrapping different species in ion traps using multiple radio frequencies", Physical Review A **94**, 023609 (2016).

[31] Z. Meir, "Dynamics of a single, ground-state cooled and trapped ion colliding with ultracold atoms: a micromotion tale.", PhD thesis (2016).

[32] E. Mathieu, "Mémoire sur le mouvement vibratoire d'une membrane de forme elliptique.", Journal de Mathématiques Pures et Appliquées **13**, 137–203.

[33] D. J. Wineland, C. Monroe, W. M. Itano, D. Leibfried, B. E. King, and D. M. Meekhof, "Experimental issues in coherent quantum-state manipulation of trapped atomic ions", Journal of research of the National Institute of Standards and Technology **103**, 259 (1998).

Appendix A

Code for Simulation of Dual-frequency

A.1 Simulation of one ion in a trap

```
# %%
import numpy as np
import matplotlib.pyplot as plt
import math
import scipy as sp
from scipy.integrate import odeint
from math import pi
import time
from scipy.fft import rfft, rfftfreq,fft, fftfreq

# %%
def dvdt(input, t, a):
    x, vx, y, vy, z, vz = input
    a = [vx,-x*(a[0][0]+2*a[1][0]*np.cos(a[2]*t))*((a[2])**2)/4,
         vy,-y*(a[0][1]+2*a[1][1]*np.cos(a[2]*t))*((a[2])**2)/4,
         vz,-z*(a[0][2]+2*a[1][2]*np.cos(a[2]*t))*((a[2])**2)/4]
    return a

# %%
t0 = np.linspace(0, 1e-3, 100000)  # [sec] time of simulation

#[[a_x,a_y,a_z],[q_x,q_y,q_z],Omega]
a = [[-0.001,-0.001,0.002],[-0.1,0.1,0],2*np.pi*26.5*1e6]

y0 = [8e-10,0,8e-10,0,8e-10,0] #[x0,vx0,y0,vy0,z0,vz0], intial
    conditions = [x position, x velocity, y position, ...]

st = time.time()
```

```
28 sol = odeint(dvdt, y0, t0, args = (a,)) #solver
29 et = time.time()
30
31 # %%
32 # results:
33 xt = sol[:, 0]  # x(t) [m]
34 vxt = sol[:, 1]  # vx(t) [m/s]
35
36 yt = sol[:, 2]  # y(t) [m]
37 vyt = sol[:, 3]  # vy(t) [m/s]
38
39 zt = sol[:, 4]  # z(t) [m]
40 vzt = sol[:, 5]  # vz(t) [m/s]
41
42 # plotting:
43 plt.figure()
44 fig = plt.figure(figsize=(15,6))
45 plt.title("Single ion position vs time using Odeint")
46 plt.xlim(0,5)
47 plt.plot(t0*1e6, xt*1e9, '-', label='numeric x')
48 plt.plot(t0*1e6, yt*1e9, '-', label='numeric y')
49 plt.plot(t0*1e6, zt*1e9, '-', label='numeric z')
50
51 plt.xlabel('t [us]')
52 plt.ylabel('ui [nm]')
53 plt.legend()
54 plt.savefig("position_vs_time_using_Odeint")
55
56 plt.show()
57
58 # %%
59 #analytical solution
60 A = [8.4e-10,7.6e-10,8e-10]
61
62 q = np.array([-0.1,0.1,0])
63 a = np.array([-0.001,-0.001,0.002])
64 Omega = 26.5*1e6
65
66 omega =  (Omega/2)*np.sqrt(a+(q**2)/2)
67
68 x = []
69 y = []
70 z = []
71
72 for t in t0:
73     x.append(A[0]*(np.cos(omega[0]*2*pi*t)*(1+(q[0]/2)*np.cos(
    Omega*2*pi*t)+((q[0]**2)/32)*np.cos(2*Omega*2*pi*t))+(omega[0]/
    Omega)*q[0]*np.sin(omega[0]*2*pi*t)*np.sin(Omega*2*pi*t)))
```

```
74      y.append(A[1]*(np.cos(omega[1]*2*pi*t)*(1+(q[1]/2)*np.cos(
        Omega*2*pi*t)+((q[1]**2)/32)*np.cos(2*Omega*2*pi*t))+(omega[1]/
        Omega)*q[1]*np.sin(omega[1]*2*pi*t)*np.sin(Omega*2*pi*t)))
75      z.append(A[2]*(np.cos(omega[2]*2*pi*t)*(1+(q[2]/2)*np.cos(
        Omega*2*pi*t)+((q[2]**2)/32)*np.cos(2*Omega*2*pi*t))+(omega[2]/
        Omega)*q[2]*np.sin(omega[2]*2*pi*t)*np.sin(Omega*2*pi*t)))
76
77  x = np.array(x)
78  y = np.array(y)
79  z = np.array(z)
80
81  # %%
82  #comparison between analytical and computational solution
83
84  fig, ax = plt.subplots(1,3, figsize=(24, 4))
85  fig. suptitle("Single ion, Comparison between analytical and
        computational solution using odeint", fontsize=15)
86
87
88  ax[0].plot(t0*1e6,x*1e9, label="Analytical")
89  ax[0].plot(t0*1e6,xt*1e9, label="Numerical")
90  ax[0].legend(loc='upper left')
91  ax[0].set_ylabel('t [us]')
92  ax[0].set_xlabel('x[nm]')
93  ax[0].set_xlim(0,3)
94
95
96
97  ax[1].plot(t0*1e6,y*1e9, label="Analytical")
98  ax[1].plot(t0*1e6,yt*1e9, label="Numerical")
99  ax[1].legend(loc='upper left')
100 ax[1].set_ylabel('t [us]')
101 ax[1].set_xlabel('y[nm]')
102 ax[1].set_xlim(0,3)
103
104
105 ax[2].plot(t0*1e6,z*1e9, label="Analytical")
106 ax[2].plot(t0*1e6,zt*1e9, label="Numerical")
107 ax[2].legend(loc='upper left')
108 ax[2].set_ylabel('t [us]')
109 ax[2].set_xlabel('z[nm]')
110 ax[2].set_xlim(0,3)
111
112
113 ax[0].set_title("x position")
114 ax[1].set_title("y position")
115 ax[2].set_title("z position")
116
117 plt.savefig("Analytical_vs_computational_Odeint")
```

```
118
119
120 # %%
121 q = np.array([-0.1,0.1,0])
122 a = np.array([-0.001,-0.001,0.002])
123 Omega = 26.5*1e6 #rf frequency
124 #secular frequency
125 omega =  (Omega/2)*np.sqrt((a+(q**2)*(0.5+(a/8))+(q**4)/128)/(1-(q
    **2)*((3/8)+(5*a/16))))
126
127 # %%
128 # FFT:
129
130 N = len(xt)
131 xf = rfft(xt)
132 yf = rfft(yt)
133 zf = rfft(zt)
134 sample_rate = 1/(t0[1]-t0[0])  # [Hz]
135 xrf = rfftfreq(N, 1/sample_rate)
136
137 plt.figure()
138 fig = plt.figure(figsize=(10,6))
139
140 plt.plot(xrf,np.abs(xf),label = "x")
141
142 # plt.plot(xrf,np.abs(yf),label = "y")
143 # plt.plot(xrf,np.abs(zf),label = "z")
144 plt.plot(omega[0]*np.array([1,1]), [0,np.max(np.abs(xf))],'--',
    label = "$\\omega$ (Secular frequqncy)")
145 plt.plot((omega[0]+Omega)*np.array([1,1]), [0,0.032*np.max(np.abs(
    xf))],'--',label = "$\\Omega +\\omega$")
146 plt.plot((-omega[0]+Omega)*np.array([1,1]), [0,0.035*np.max(np.abs
    (xf))],'--',label = "$\\Omega - \\omega$")
147 plt.legend()
148 # plt.xlim(0.7e6, 0.875e6)
149 # plt.xlim(2.725e7, 2.74e7)
150 # plt.ylim(-0.01e-5,0.125e-5)
151
152 # print(omega[0], Omega)
153
154 plt.title('Spectrum')
155 plt.xlabel('Frequency[Hz]')
156 plt.ylabel('Amplitude')
157 plt.savefig("FT_single_ion_position_vs_time_using_Odeint")
158
159 plt.show()
```

A.2 Simulation of two ions in a trap

```
# %%
import numpy as np
import matplotlib.pyplot as plt
import math
import scipy as sp
from scipy.integrate import odeint
from math import pi
import time
from scipy.fft import rfft, rfftfreq,fft, fftfreq

# %%
#starting from random position
# t = 0
q_a = 1.6e-19 #charge of a
q_b = 1.6e-19  #charge of b
m_a = 40*1.672621898e-27 #mass of a
m_b = 28*1.672621898e-27 #mass of b

#constant for the coloumbic force
const_a = q_a*q_b/(m_a*4*pi*8.854187817*1e-12)
const_b = q_a*q_b/(m_b*4*pi*8.854187817*1e-12)

#other parameters
e = 1.60217663e-19
v_dc = 500
v_rf = 500
O = 24*2*np.pi*1e6
Z_0 = 9.04*1e-3
R_0 = 0.716*1e-3

#for mass a
a_xa = (-4*e*v_dc)/(m_a*(O**2)*(Z_0**2))
a_ya = a_xa
a_za = -2*a_xa

q_xa = (2*e*v_rf)/(m_a*(O**2)*(R_0**2))
q_ya = -q_xa
q_za = 0


#for mass b
a_xb = (-4*e*v_dc)/(m_b*(O**2)*(Z_0**2))
a_yb = a_xb
a_zb = -2*a_xb

q_xb = (2*e*v_rf)/(m_b*(O**2)*(R_0**2))
```

```
47 q_yb = -q_xb
48 q_zb = 0
49
50 #defining all 'a' and 'q' values for both masses in as a list
51 aq0 = [[a_xa,a_ya,a_za],[q_xa,q_ya,q_za],0,[a_xb,a_yb,a_zb],[q_xb,
       q_yb,q_zb]]
52
53 #to get initial positions of ions
54 # wx_a =  (aq0[2]/2)*np.sqrt(aq0[0][0]+(aq0[1][0]**2)/2)
55 # wy_a =  (aq0[2]/2)*np.sqrt(aq0[0][1]+(aq0[1][1]**2)/2)
56 wz_a =  (aq0[2]/2)*np.sqrt(aq0[0][2]+(aq0[1][2]**2)/2)
57
58 # wx_b =  (aq0[2]/2)*np.sqrt(aq0[3][0]+(aq0[4][0]**2)/2)
59 # wy_b =  (aq0[2]/2)*np.sqrt(aq0[3][1]+(aq0[4][1]**2)/2)
60 wz_b =  (aq0[2]/2)*np.sqrt(aq0[3][2]+(aq0[4][2]**2)/2)
61
62 r_a = np.cbrt(q_a*q_b/(2*np.pi*8.854187817*1e-12*(m_a)*(wz_a**2)))
63 r_b = np.cbrt(q_a*q_b/(2*np.pi*8.854187817*1e-12*(m_b)*(wz_b**2)))
64
65 # initial conditions = [x0_a,vx0_a,y0_a,vy0_a,z0_a,vz0_a,x0_b,
       vx0_b,y0_b,vy0_b,z0_b,vz0_b]
66 y0 = [1e-9,0.0,1e-9,0.0,1e-9+r_a/2,0.0,1e-9,0.0,1e-9,0.0,1e-9-r_b
       /2,0.0]
67
68 # %%
69 print(r_a,r_b)
70
71 # %%
72 def dvdt(input, t, a):
73     x_a, vx_a, y_a, vy_a, z_a, vz_a, x_b, vx_b, y_b, vy_b, z_b,
       vz_b  = input
74
75     r_ab = np.sqrt(((x_a-x_b)**2)+((y_a-y_b)**2)+((z_a-z_b)**2))
76
77     a = [vx_a,-(x_a*(a[0][0]+2*a[1][0]*np.cos(a[2]*t))*(a[2]**2)
       /4)+const_a*(x_a-x_b)/r_ab**3,
78          vy_a,-(y_a*(a[0][1]+2*a[1][1]*np.cos(a[2]*t))*(a[2]**2)
       /4)+const_a*(y_a-y_b)/r_ab**3,
79          vz_a,-(z_a*(a[0][2]+2*a[1][2]*np.cos(a[2]*t))*(a[2]**2)
       /4)+const_a*(z_a-z_b)/r_ab**3,
80
81          vx_b,-(x_b*(a[3][0]+2*a[4][0]*np.cos(a[2]*t))*(a[2]**2)
       /4)+const_b*(x_b-x_a)/r_ab**3,
82          vy_b,-(y_b*(a[3][1]+2*a[4][1]*np.cos(a[2]*t))*(a[2]**2)
       /4)+const_b*(y_b-y_a)/r_ab**3,
83          vz_b,-(z_b*(a[3][2]+2*a[4][2]*np.cos(a[2]*t))*(a[2]**2)
       /4)+const_b*(z_b-z_a)/r_ab**3]
84     return a
85
```

```
86 # %%
87 t0 = np.linspace(0, 1e-3, 100000)
88
89 st = time.time()
90 sol = odeint(dvdt, y0, t0, args = (aq0,))
91 et = time.time()
92
93 # %%
94 # results:
95 xt_a = sol[:, 0]  # x(t) [m]
96 vxt_a = sol[:, 1]  # vx(t) [m/s]
97
98 yt_a = sol[:, 2]  # y(t) [m]
99 vyt_a = sol[:, 3]  # vy(t) [m/s]
100
101 zt_a = sol[:, 4]  # z(t) [m]
102 vzt_a = sol[:, 5]  # vz(t) [m/s]
103
104 xt_b = sol[:, 6]  # x(t) [m]
105 vxt_b = sol[:, 7]  # vx(t) [m/s]
106
107 yt_b = sol[:, 8]  # y(t) [m]
108 vyt_b = sol[:, 9]  # vy(t) [m/s]
109
110 zt_b = sol[:, 10]  # z(t) [m]
111 vzt_b = sol[:, 11]  # vz(t) [m/s]
112
113 # plotting:
114 plt.figure()
115 fig = plt.figure(figsize=(10,6))
116 plt.suptitle("Radial in-phase modes for two ions with smaller mass
      difference")
117 # plt.title("Radial in phase modes")
118 plt.xlim(0,10)
119 plt.plot(t0*1e6, xt_a*1e9, '-', label='numeric x_a')
120 plt.plot(t0*1e6, yt_a*1e9, '-', label='numeric y_a')
121 plt.plot(t0*1e6, zt_a*1e9-r_a*1e9/2, '-', label='numeric z_a')
122 plt.plot(t0*1e6, xt_b*1e9, '-', label='numeric x_b')
123 plt.plot(t0*1e6, yt_b*1e9, '-', label='numeric y_b')
124 plt.plot(t0*1e6, zt_b*1e9+r_b*1e9/2, '-', label='numeric z_b')
125
126 plt.xlim(0,5)
127 plt.xlabel('t [us]')
128 plt.ylabel('ui [nm]')
129 plt.legend()
130 # plt.savefig("
     two_ions_diff_mass_position_vs_time_using_Odeint_radial_out_phase
     ")
131
```

```
plt.show()

# %%
#plotting two ions

fig, ax = plt.subplots(1,3, figsize=(20, 4))
# fig. suptitle("Out of phase modes for two ions with same mass",
    fontsize=15)
fig. suptitle("In-phase modes for two ions with smaller difference
    in their masses", fontsize=15)




ax[0].plot(t0*1e6,xt_a*1e9, label="$Ca^+$")
ax[0].plot(t0*1e6,xt_b*1e9, label="$N_2^+$")
ax[0].legend(loc='upper left')
ax[0].set_ylabel('t [us]')
ax[0].set_xlabel('x[nm]')
ax[0].set_xlim(0,3)



ax[1].plot(t0*1e6,yt_a*1e9, label="$Ca^+$")
ax[1].plot(t0*1e6,yt_b*1e9, label="$N_2^+$")
ax[1].legend(loc='upper left')
ax[1].set_ylabel('t [us]')
ax[1].set_xlabel('y[nm]')
ax[1].set_xlim(0,3)


ax[2].plot(t0*1e6,zt_a*1e9-r_a*1e9/2, label="$Ca^+$")
ax[2].plot(t0*1e6,zt_b*1e9+r_b*1e9/2, label="$N_2^+$")
ax[2].legend(loc='upper left')
ax[2].set_ylabel('t [us]')
ax[2].set_xlabel('z[nm]')
ax[2].set_xlim(0,3)
ax[2].set_ylim(1.5,-1.5)

ax[0].set_title("Radial motion(x-axis)")
ax[1].set_title("Rdial motion(y-axis)")
ax[2].set_title("Axial motion(z-axis)")

plt.savefig("
    two_ions_diff_mass_position_vs_time_using_Odeint_in_phase")



# %%
```

```
178
179 # FFT:
180 N = len(xt_a)
181 #mass a
182 xf_a = rfft(xt_a)
183 yf_a = rfft(yt_a)
184 zf_a = rfft(zt_a-r_a/2)
185
186 #mass b
187 xf_b = rfft(xt_b)
188 yf_b = rfft(yt_b)
189 zf_b = rfft(zt_b+r_a/2)
190
191 sample_rate = 1/(t0[1]-t0[0])  # [Hz]
192 xrf = rfftfreq(N, 1/sample_rate)
193
194
195 # %%
196 plt.figure()
197 fig = plt.figure(figsize=(10,6))
198
199 plt.plot(xrf,np.abs(xf_a),label = "x_a")
200 plt.plot(xrf,np.abs(yf_a),label = "y_a")
201 plt.plot(xrf,np.abs(zf_a),label = "z_a")
202
203 plt.plot(xrf,np.abs(xf_b),label = "x_b")
204 plt.plot(xrf,np.abs(yf_b),label = "y_b")
205 plt.plot(xrf,np.abs(zf_b),label = "z_b")
206
207
208 plt.legend()
209 # plt.xlim(0,3e7)
210
211
212 fig.suptitle('Two ions, Different mass')
213 plt.title("Fourier transform of motion")
214
215 plt.xlabel('Frequency[Hz]')
216 plt.ylabel('Amplitude')
217
218 plt.savefig("FT_two_ions_diff_mass_position_vs_time_using_Odeint")
219 plt.show()
220
221 # %%
222 Omega = 24*1e6
223
224 aa = np.array([a_xa, a_ya, a_za])
225 qa = np.array([q_xa,q_ya,q_za])
226 ab = np.array([a_xb, a_yb, a_zb])
```

```
227 qb = np.array([q_xb,q_yb,q_zb])
228
229 # # two same masses
230 # omega =  ((O/2)*np.sqrt(((qa**2)/2) + aa))/(2*np.pi) #in-phase
231 # omega =  ((O/2)*np.sqrt(((qa**2)/2) + 3*aa))/(2*np.pi) #out-of-
    phase
232
233 #two different masses
234 mu = m_a/m_b
235
236 #dror
237 omega_ip_a = (O*np.sqrt(np.abs(((qa**2)+(qb**2)+4*aa*(1-mu)-np.
    sqrt(((qa**2+4*aa)-(qb**2+4*ab))**2+(4*aa)**2*mu))/16)))/(2*np.
    pi) #in-phase
238 omega_op_a =  (O*np.sqrt((qa**2+qb**2+4*aa*(1+mu)+np.sqrt(((qa
    **2+4*aa)-(qb**2+4*ab))**2+(4*aa)**2*mu))/16))/(2*np.pi) #out-
    of-phase
239
240 # #morigi
241 # omega_ip_a = wz_a*np.sqrt(1+(1/mu)+np.sqrt(1+(1/(mu**2))-(1/mu))
    )
242 # omega_op_a = wz_a*np.sqrt(1+(1/mu)-np.sqrt(1+(1/(mu**2))-(1/mu))
    )
243
244
245 # %%
246 plt.figure()
247 fig = plt.figure(figsize=(10,6))
248
249 # plt.plot(xrf,np.abs(zf_a),label = "z_a")
250
251
252 plt.plot(xrf,np.abs(zf_b),label = "z_b")
253 plt.plot(xrf,np.abs(zf_a),label = "z_a")
254
255 #dror
256 plt.plot((omega_op_a[2])*np.array([1,1]), [0,0.15*np.max(np.abs(
    zf_a))],'--',label = "$\\omega$ (Secular frequqncy)")
257 plt.plot((omega_ip_a[2])*np.array([1,1]), [0,np.max(np.abs(zf_a))
    ],'--',label = "$\\Omega +\\omega$")
258
259 #morigi
260 # plt.plot((omega_op_a)*np.array([1,1]), [0,np.max(np.abs(zf_a))
    ],'--',label = "$\\omega$ (Secular frequqncy)")
261 # plt.plot((omega_ip_a)*np.array([1,1]), [0,np.max(np.abs(xf_a))
    ],'--',label = "$\\Omega +\\omega$")
262
263
264 plt.legend()
```

```
265
266
267 fig.suptitle('Two ions, Different mass')
268 plt.title("Fourier transform of motion")
269 # plt.xlim(0,2e6)
270 plt.xlabel('Frequency[Hz]')
271 plt.ylabel('Amplitude')
272 plt.savefig("FT_two_ions_diff_mass_position_vs_time_using_Odeint")
273 plt.show()
274
275 # %%
276 plt.figure()
277 fig = plt.figure(figsize=(10,6))
278
279 plt.plot(xrf,np.abs(xf_a),label = "x_a")
280
281
282 plt.plot(xrf,np.abs(xf_b),label = "x_b")
283
284 plt.plot(omega_op_a[0]*np.array([1,1]), [0,np.max(np.abs(zf_a))],'
    --',label = "$\\omega$ (Secular frequqncy)")
285 plt.plot((omega_op_a[0]+Omega)*np.array([1,1]), [0,0.035*np.max(np
    .abs(xf_a))],'--',label = "$\\Omega +\\omega$")
286 plt.plot((-omega_op_a[0]+Omega)*np.array([1,1]), [0,0.07*np.max(np
    .abs(xf_a))],'--',label = "$\\Omega - \\omega$")
287
288 plt.plot(omega_ip_a[0]*np.array([1,1]), [0,np.max(np.abs(zf_a))],'
    --',label = "$\\omega$ (Secular frequqncy)")
289 plt.plot((omega_ip_a[0]+Omega)*np.array([1,1]), [0,0.035*np.max(np
    .abs(xf_a))],'--',label = "$\\Omega +\\omega$")
290 plt.plot((-omega_ip_a[0]+Omega)*np.array([1,1]), [0,0.07*np.max(np
    .abs(xf_a))],'--',label = "$\\Omega - \\omega$")
291
292
293 plt.legend()
294 # plt.xlim(0,3e7)
295
296
297 fig.suptitle('Two ions, Different mass')
298 plt.title("Fourier transform of motion")
299
300 plt.xlabel('Frequency[Hz]')
301 plt.ylabel('Amplitude')
302
303 plt.savefig("FT_two_ions_diff_mass_position_vs_time_using_Odeint")
304 plt.show()
```

A.3 Simulation of two ions in Dual-frequency Paul trap

```
# %%
import numpy as np
import matplotlib.pyplot as plt
import math
import scipy as sp
from scipy.integrate import odeint
from math import pi
import time
from scipy.fft import rfft, rfftfreq,fft, fftfreq

# %%
#starting from random position
# t = 0
q_a = 1.6e-19 #charge on ion a
q_b = 1.6e-19 #charge on ion b
m_a = 40*1.672621898e-27  #mass of ion a
m_b = 254*1.672621898e-27 #mass of ion b

const_a = q_a*q_b/(m_a*4*pi*8.854187817*1e-12)   #coloumb force
const_b = q_a*q_b/(m_b*4*pi*8.854187817*1e-12)

e = 1.60217663e-19  # electron charge
v_dc = 500          # DC Voltage
v_rf1 = 500          # RF voltage
v_rf2 = 500          # RF voltage

O_1 = 24*2*np.pi*1e6  # Frequency at which RF Voltage is applied
O_2 = 24.0011*2*np.pi*1e6  # Frequency at which RF Voltage is
    applied

Z_0 = 9.04*1e-3     # Effective center-of-trap-electrode distance
R_0 = 0.716*1e-3    # Distance between center of the trap and the
    electrode

#for mass a
a_xa = (-4*e*v_dc)/(m_a*(Z_0**2)*(O_1**2))
a_ya = a_xa
a_za = -2*a_xa

q_xa1 = -(2*e*v_rf1)/(m_a*2*(R_0**2)*(O_1**2))
q_ya1 = -q_xa1
q_za1 = 0

q_xa2 = -(2*e*v_rf2)/(m_a*2*(R_0**2)*(O_2**2))
q_ya2 = -q_xa2
```

```
q_za2 = 0


#for mass b
a_xb = (-4*e*v_dc)/(m_b*(Z_0**2)*(O_1**2))
a_yb = a_xb
a_zb = -2*a_xb

q_xb1 = (2*e*v_rf1)/(m_b*2*(R_0**2)*(O_1**2))
q_yb1 = -q_xb1
q_zb1 = 0

q_xb2 = (2*e*v_rf2)/(m_b*2*(R_0**2)*(O_2**2))
q_yb2 = -q_xb2
q_zb2 = 0

aq0 = [[a_xa,a_ya,a_za],[q_xa1,q_ya1,q_za1],[q_xa2,q_ya2,q_za2],
    O_1,[a_xb,a_yb,a_zb],[q_xb1,q_yb1,q_zb1],[q_xb2,q_yb2,q_zb2],
    O_2]


# wx_a =  (aq0[3]/2)*np.sqrt(aq0[0][0]+(aq0[1][0]**2)/2)
# wy_a =  (aq0[3]/2)*np.sqrt(aq0[0][1]+(aq0[1][1]**2)/2)
wz_a =  (aq0[3]/2)*np.sqrt(aq0[0][2]+(aq0[1][2]**2)/2)

# wx_b =  (aq0[3]/2)*np.sqrt(aq0[4][0]+(aq0[5][0]**2)/2)
# wy_b =  (aq0[3]/2)*np.sqrt(aq0[4][1]+(aq0[5][1]**2)/2)
wz_b =  (aq0[3]/2)*np.sqrt(aq0[4][2]+(aq0[5][2]**2)/2)

r_a = np.cbrt(q_a*q_b/(2*np.pi*8.854187817*1e-12*(m_a)*(wz_a**2)))
r_b = np.cbrt(q_a*q_b/(2*np.pi*8.854187817*1e-12*(m_b)*(wz_b**2)))

# initial conditions = [x0_a,vx0_a,y0_a,vy0_a,z0_a,vz0_a,x0_b,
    vx0_b,y0_b,vy0_b,z0_b,vz0_b]
y0 = [1e-9,0.0,0.0,0.0,1e-9+r_a/2,0.0,0.0,0.0,0.0,0.0,-r_b/2,0.0]

# %%
r_a

# %%
def dvdt(input, t, a):
    x_a, vx_a, y_a, vy_a, z_a, vz_a, x_b, vx_b, y_b, vy_b, z_b,
    vz_b  = input

    r_ab = np.sqrt(((x_a-x_b)**2)+((y_a-y_b)**2)+((z_a-z_b)**2))

    a = [vx_a,-(x_a*(((a[3]**2)/4)*a[0][0]+((a[3]**2)/4)*2*a
    [1][0]*np.cos(a[3]*t)+((a[7]**2)/4)*2*a[2][0]*np.cos(a[7]*t)))+
    const_a*(x_a-x_b)/r_ab**3,
```

```
87          vy_a,-(y_a*(((a[3]**2)/4)*a[0][1]+((a[3]**2)/4)*2*a
    [1][1]*np.cos(a[3]*t)+((a[7]**2)/4)*2*a[2][1]*np.cos(a[7]*t)))+
    const_a*(y_a-y_b)/r_ab**3,
88          vz_a,-(z_a*(((a[3]**2)/4)*a[0][2]+((a[3]**2)/4)*2*a
    [1][2]*np.cos(a[3]*t)+((a[7]**2)/4)*2*a[2][2]*np.cos(a[7]*t)))+
    const_a*(z_a-z_b)/r_ab**3,
89
90          vx_b,-(x_b*(((a[3]**2)/4)*a[4][0]+((a[3]**2)/4)*2*a
    [5][0]*np.cos(a[3]*t)+((a[7]**2)/4)*2*a[6][0]*np.cos(a[7]*t)))+
    const_b*(x_b-x_a)/r_ab**3,
91          vy_b,-(y_b*(((a[3]**2)/4)*a[4][1]+((a[3]**2)/4)*2*a
    [5][1]*np.cos(a[3]*t)+((a[7]**2)/4)*2*a[6][1]*np.cos(a[7]*t)))+
    const_b*(y_b-y_a)/r_ab**3,
92          vz_b,-(z_b*(((a[3]**2)/4)*a[4][2]+((a[3]**2)/4)*2*a
    [5][2]*np.cos(a[3]*t)+((a[7]**2)/4)*2*a[6][2]*np.cos(a[7]*t)))+
    const_b*(z_b-z_a)/r_ab**3]
93      return a
94
95  # %%
96  t0 = np.linspace(0, 1e-4, 10000)
97
98  st = time.time()
99  sol = odeint(dvdt, y0, t0, args = (aq0,))
100 et = time.time()
101
102 # %%
103 # results:
104 xt_a = sol[:, 0]  # x(t) [m]
105 vxt_a = sol[:, 1]  # vx(t) [m/s]
106
107 yt_a = sol[:, 2]  # y(t) [m]
108 vyt_a = sol[:, 3]  # vy(t) [m/s]
109
110 zt_a = sol[:, 4]  # z(t) [m]
111 vzt_a = sol[:, 5]  # vz(t) [m/s]
112
113 xt_b = sol[:, 6]  # x(t) [m]
114 vxt_b = sol[:, 7]  # vx(t) [m/s]
115
116 yt_b = sol[:, 8]  # y(t) [m]
117 vyt_b = sol[:, 9]  # vy(t) [m/s]
118
119 zt_b = sol[:, 10]  # z(t) [m]
120 vzt_b = sol[:, 11]  # vz(t) [m/s]
121
122 # plotting:
123 plt.figure()
124 fig = plt.figure(figsize=(15,6))
125 # plt.suptitle("two ions with large mass difference")
```

```
126 plt.title("Two ions with large mass differences")
127 # plt.xlim(0,30)
128 # plt.plot(t0*1e6, xt_a*1e6, '-', label=r'$Ca^+$ in x')
129 # plt.plot(t0*1e6, yt_a*1e6, '-', label='$Ca^+$ in y')
130 # plt.plot(t0*1e6, (zt_a-r_a/2)*1e6, '-', label='$Ca^+$ in z')
131 # plt.plot(t0*1e6, xt_b*1e6, '-', label='$I_2^+$ in x')
132 # plt.plot(t0*1e6, yt_b*1e6, '-', label='$I_2^+$ in y')
133 # plt.plot(t0*1e6, (zt_b+r_b/2)*1e6, '-', label='$I_2^+$ in z')
134
135
136 plt.plot(t0*1e6, xt_a, '-', label=r'$Ca^+$ in x')
137 plt.plot(t0*1e6, yt_a, '-', label='$Ca^+$ in y')
138 plt.plot(t0*1e6, (zt_a-r_a/2), '-', label='$Ca^+$ in z')
139 plt.plot(t0*1e6, xt_b, '-', label='$I_2^+$ in x')
140 plt.plot(t0*1e6, yt_b, '-', label='$I_2^+$ in y')
141 plt.plot(t0*1e6, (zt_b+r_b/2), '-', label='$I_2^+$ in z')
142
143 # plt.xlim(0,40)
144 plt.xlabel('Time [$\mu$s]')
145 plt.ylabel('Position [$\mu$m]')
146 plt.legend()
147 plt.savefig("teo_ions_diff_mass_position_vs_time_using_Odeint")
148
149 plt.show()
```

Appendix B

Meme

This was me to Idan every other day(source Instagram)